Title: Maturing Mycobacterial Peptidoglycan Required Non-canonical Crosslinks to Maintain Shape

Authors: Catherine Baranowski[1], Lok-To Sham[2,3], Haig A. Eskandarian[4,5], Michael A. Welsh[2], Hoong C. Lim[2], Karen J. Kieser[1], Jeffrey C. Wagner[1], Suzanne Walker[2], John D. McKinney[4], Georg E. Fantner[5], Thomas R. Ioerger[6], Thomas G. Bernhardt[2], Eric J. Rubin[1,2]*, E. Hesper Rego[7*]

Affiliations:

[1] Department of Immunology and Infectious Disease, Harvard T. H. Chan School of Public Health, Boston, MA 02115, USA.

[2] Department of Microbiology and Immunobiology, Harvard Medical School, Boston, MA 02115, USA.

[3] Department of Microbiology and Immunology, National University of Singapore, 117545 Singapore.

[4] School of Life Sciences, Swiss Federal Institute of Technology in Lausanne (EPFL), 1015 Lausanne, Switzerland.

[5] School of Engineering, Swiss Federal Institute of Technology in Lausanne (EPFL), 1015 Lausanne, Switzerland.

[6]Department of Computer Science and Engineering, Texas A&M University, College Station, Texas, USA.

[7] Department of Microbial Pathogenesis, Yale University School of Medicine, New Haven, Connecticut, 06510, USA.

* to whom correspondence should be addressed: erubin@hsph.harvard.edu; hesper.rego@yale.edu

Abstract:

In most well-studied rod-shaped bacteria, peptidoglycan is primarily crosslinked by penicillin binding proteins (PBPs). However, in mycobacteria L,D-transpeptidase (LDT)-mediated crosslinks are highly abundant. To elucidate the role of these unusual crosslinks, we characterized mycobacterial cells lacking all LDTs. We find that LDT-mediated crosslinks are required for rod shape maintenance specifically at sites of aging cell wall, a byproduct of polar elongation. Asymmetric polar growth leads to a non-uniform distribution of these two types of crosslinks in a single cell. Consequently, in the absence of LDT-mediated crosslinks, PBP-catalyzed crosslinks become more important. Because of this, *Mycobacterium tuberculosis* is more rapidly killed using a combination of drugs capable of PBP and LDT inhibition. Thus, knowledge about the single-cell distribution of drug targets can be exploited to more effectively treat this pathogen.

One Sentence Summary: Polar elongating mycobacteria utilize specific cell wall chemistry to maintain rod shape at sites of aging cell wall.

Main Text:

Peptidoglycan (PG) is an essential component of all bacterial cells (*1*), and the target of many antibiotics. PG consists of linear glycan strands crosslinked by short peptides to form a continuous molecular cage surrounding the plasma membrane. This structure maintains cell shape and protects the plasma membrane from rupture. Our understanding of PG is largely

derived from studies on laterally-growing model rod-shaped bacteria like *Escherichia coli* and *Bacillus subtilis* (Fig. S1A). However, there are important differences between these bacteria and the mycobacteria, a genus that includes the major human pathogen *Mycobacterium tuberculosis* (Mtb). In mycobacteria, new PG is inserted at the cell poles (at unequal amounts based on pole age), rather than along the lateral side walls (Fig. 1A). In addition, in model rod-shaped bacteria like *E. coli*, PBP-mediated crosslinks make up a vast majority of the PG linkages (*2*). PBPs, the targets of most β-lactams, catalyze peptide links between PG strands, forming 4-3 crosslinks (Fig. S1B). However, in mycobacteria, 3-3 crosslinks, formed by L,D-transpeptidases (LDTs), are abundant (~60% of linkages (*3*)) (Fig. S1B). Because PG has been most well studied in bacteria where 3-3 crosslinks are rare, the role of this linkage - and the enzymes that catalyze it - is poorly understood. Importantly, carbapenems, β-lactam antibiotics that potently inhibit LDTs *in vitro*, are effective against Mtb *in vitro* and in patients (*4*, *5*). Thus, we sought to understand the role of 3-3 crosslinks in mycobacterial physiology.

PG uniquely contains D-amino acids which can be labeled with fluorescent probes (fluorescent D-amino acids, FDAAs) to visualize PG synthesis in live bacterial cells (*6*). When we incubated Msm with FDAAs for a short 2-minute pulse (< 2% of Msm's generation time) we observed incorporation at both poles, the sites of new PG insertion in mycobacteria (Fig. 1A) (*7*). However, we also saw a gradient extending from the old pole (the previously established growth pole) that fades to a minimum at roughly mid-cell as it reaches the new pole (the pole formed at the last cell division) (Fig. 1B).

To identify the enzymes responsible for this unexpected pattern of lateral cell wall FDAA incorporation, we performed a fluorescence-activated cell sorting (FACS)-based transposon screen (Fig. S1C). Briefly, we stained an Msm transposon library with FDAA and repeatedly sorted the

least fluorescent 12.5% of the population by FACS. After each sort we regrew cells, extracted gDNA and used deep sequencing to map the location of the transposons found in the low staining population.

From this screen, we identified three LDTs (*ldtA-MSMEG_3528, ldtB-MSMEG_4745, ldtE-MSMEG_0233*) (Fig. S1D) that were primarily responsible for FDAA incorporation. Deleting these three LDTs significantly reduced FDAA incorporation (Fig. S2A,B). To further investigate the physiological role of LDTs, we constructed a strain lacking all 6 LDTs (Δ*ldtAEBCGF*, hereafter ΔLDT). FDAA incorporation and 3-3 crosslinking is nearly abolished in ΔLDT cells and can be partially restored by complementation with a single LDT (*ldtE*-mRFP; ΔLDT_{comp}) (Fig. 1C, S2C,D, S3). Thus, like *Bdellovibrio* (*6*, *8*), FDAA incorporation in Msm is primarily LDT-dependent. LDTs can also exchange non-canonical D-amino acids onto PG tetrapeptides in *Vibrio cholera* (*9*).

As partial knock-outs of LDTs in Msm have morphologic changes (*10*), we visualized ΔLDT cells by time-lapse microscopy. We observed that a subpopulation of cells loses rod shape progressively over time, resulting in localized spherical blebs (Fig. 2A-top, S4A). Complemented cells are able to maintain rod shape (Fig. S4B). We reasoned that localized loss of rod shape may occur for two reasons: 1) spatially-specific loss of cell wall integrity and/or 2) cell wall deformation due to uncontrolled, local PG synthesis. If the first hypothesis, were true, high osmolarity should protect cells against forming blebs. Indeed, switching cells from iso- to high-osmolarity prevented bleb formation over time (Fig. 2A, bottom). These results indicate that 3-3 crosslinks are required to counteract turgor pressure and maintain the rod shape of mycobacteria. To test the second hypothesis, we stained ΔLDT cells with an amine-reactive dye, and observed outgrowth of new, unstained material (Fig. 2B). Blebs retained stain, indicating a lack of new PG

synthesis in the region. We, therefore, hypothesized that 3-3 crosslinks are required to maintain the structural stability necessary for the rod shape of mycobacteria.

To directly test cell wall rigidity, we used atomic force microscopy (AFM) on live ΔLDT and WT cells. We measured the rigidity of cells in relation to their height. Generally, WT cells are stiffer than ΔLDT cells (Fig. 2C). Blebs in ΔLDT cells can be identified by a sharp increase in height found toward the new pole (Fig. 2C). Since circumferential stress of the rod measured by AFM is proportional to the radius of the cell, and inversely proportional to the thickness of the cell wall (an unmeasurable quantity by AFM), we used cell height, a proxy for radius, to normalize the stiffness measurement. We found that stiffness drops in the area of blebs (Fig. 2D, pink shaded). Together, these data suggest that LDTs act locally to reinforce PG and maintain rod shape in a subpopulation of Msm cells (Fig. S4C).

Why does loss of rod shape occur only in a subpopulation of cells? Mycobacterial polar growth and division results in daughter cells with phenotypic differences (*7*). For example, the oldest cell wall is specifically inherited by the new pole daughter (Fig. S5A,(*7*)). We hypothesized that the loss of rod shape might occur in specific progeny generated by cell division. Indeed, the daughter which inherited the new pole from the previous round of division, and the oldest cell wall, consistently lost rod shape over time, while the old pole daughter maintained rod shape (Fig. S5B). In addition, blebs localized to the oldest cell wall (Fig. 2B). Thus, 3-3 crosslinking is likely occurring in the oldest cell wall, which is non-uniformly distributed in the population via asymmetric polar growth and division.

Our observations lead to the following model (Fig. 4C): PBP-catalyzed 4-3 crosslinks are formed at the poles where new PG is inserted. These newly synthesized 4-3 crosslinks are then gradually cleaved (by D-D endopeptidases) as PG ages and moves toward the middle of the cell,

leaving tetrapeptide substrates for LDTs to create 3-3 crosslinks. We can visualize this with FDAA staining which shows the distribution of tetrapeptide substrates that are progressively consumed as the cell wall ages (Fig. 1C). In the absence of LDTs, old cell wall loses integrity and turgor pressure causes bleb formation.

This model predicts that: 1) ΔLDT cells should be even more dependent on 4-3 crosslinking than wild type cells; 2) enzymes that make different types of crosslinks (PBPs vs LDTs) should be differentially localized along the length of the cell; and 3) D,D-endopeptidases, which can create LDT substrates by cleaving 4-3 crosslinks, should be localized at sites of aging PG.

To test the first prediction, we used TnSeq (*11*) to identify genes required for growth in cells lacking LDTs (Fig. 3A). We found that mutants of two PBPs, *pbpA (MSMEG_0031c)* and *ponA2 (MSMEG_6201)*, were recovered at significantly lower frequencies in ΔLDT cells (Fig. 3B). Likewise, using allele swapping (*12*) (Fig. S6A), we found that the transpeptidase activity of PonA1, which is non-essential in WT cells (*12*), becomes essential in ΔLDT cells (Fig. S6B). Thus, cells that lack 3-3 crosslinks are more dependent on 4-3 crosslinking enzymes.

To test whether 3-3 and 4-3 crosslinking enzymes localize differently, we visualized fluorescent fusions of a PBP (PonA1), and an LDT (LdtE*),* (Fig. 4A). We found that PonA1-RFP largely localized to the old pole, where new PG is inserted (Fig. 4A, B). LdtE-mRFP localized farther from the poles, the sites of older PG (Fig. 4A, B). Thus, enzymes responsible for 4-3 and 3-3 crosslinks exhibit distinctive subcellular localizations, consistent with the model that they act on differentially-aged PG

To test our third hypothesis, we sought to identify a D,D-endopeptidase in Msm and determine its subcellular localization. Using HHPRED (*13*), we identified DacB2 (MSMEG_2433), a protein shown to harbor D,D-carboxypeptidase activity in Msm (*14*), as a

candidate D,D-endopeptidase by homology to the *E. coli* protein AmpH , an enzyme with both D,D- carboxy- and endopeptidase activity (*15*). We expressed and purified DacB2 and found that it, too, had both D,D-carboxy- and D,D- endopeptidase activity on peptidoglycan substrates generated *in vitro* (Fig. S7). DacB2-mRFP localizes closer to LDT-mRFP, further from the poles, at sites of older PG (Fig. 4A, B). Thus, bleb formation may result from unchecked D,D-endopeptidase activity in ΔLDT cells.

The importance of 3-3 crosslinks in mycobacteria suggests a unique vulnerability. While mycobacteria can be killed by most non-carbapenem (N-C) β-lactams, which largely target the PBPs, carbapenems, which target both PBPs and LDTs (*16*, *17*) are also effective against *Mycobacterium tuberculosis* (*4*, *5*). As has been previously postulated (*16*, *18*, *19*), our data suggest that faster Mtb killing could be achieved with drug combinations that target both PBPs and LDTs. In fact, we find that amoxicillin (a N-C β-lactam) and meropenem (a carbapenem), in combination, exhibit synergism in minimal inhibitory concentration (Σ Fractional Inhibitory Concentration < 0.5 (*20*), Fig. S8) and lead to more rapid killing of Mtb (Fig. 3C, D, Fig. S9) (*21*).

In well-studied rod-shaped bacteria like *E.coli* and *B. subtilis*, shape is maintained by MreB-directed PG synthesis (*22-24*). Mycobacteria must maintain structural stability in the absence of an obvious MreB homolog. Further, in contrast to lateral-elongating bacteria, in which new and old cell wall are constantly intermingled during growth (Fig. S4A), polar growth segregates new and old cell wall (Fig. S10). Mycobacteria appear to utilize 3-3 crosslinks at asymmetrically-distributed aging cell wall to provide stability along the lateral body, something that may not be required in the presence of MreB-directed PG synthesis. Thus, drug combinations that target both 4-3 and 3-3 crosslinking enzymes could lead to better treatment of tuberculosis.

Interestingly, meropenem combined with amoxicillin/clavulanate resulted in early clearance of Mtb from sputum(*5*). In fact, the combination might be key to accelerated killing of Mtb.

References and Notes:

1. W. Vollmer, D. Blanot, M. A. de Pedro, Peptidoglycan structure and architecture. *FEMS Microbiol Rev*. **32**, 149–167 (2008).

2. A. G. Pisabarro, M. A. de Pedro, D. Vázquez, Structural modifications in the peptidoglycan of Escherichia coli associated with changes in the state of growth of the culture. *Journal of Bacteriology*. **161**, 238–242 (1985).

3. P. Kumar *et al.*, Meropenem inhibits D,D-carboxypeptidase activity in Mycobacterium tuberculosis. *Molecular Microbiology*. **86**, 367–381 (2012).

4. J.-E. Hugonnet, L. W. Tremblay, H. I. Boshoff, C. E. Barry, J. S. Blanchard, Meropenem-clavulanate is effective against extensively drug-resistant Mycobacterium tuberculosis. *Science*. **323**, 1215–1218 (2009).

5. A. H. Diacon *et al.*, β-Lactams against Tuberculosis--New Trick for an Old Dog? *N. Engl. J. Med.* **375**, 393–394 (2016).

6. E. Kuru *et al.*, In Situ Probing of Newly Synthesized Peptidoglycan in Live Bacteria with Fluorescent D-Amino Acids. *Angew. Chem. Int. Ed.* **51**, 12519–12523 (2012).

7. B. B. Aldridge *et al.*, Asymmetry and aging of mycobacterial cells lead to variable growth and antibiotic susceptibility. *Science*. **335**, 100–104 (2012).

8. E. Kuru *et al.*, Fluorescent D-amino-acids reveal bi-cellular cell wall modifications important for Bdellovibrio bacteriovorus predation. *Nat Microbiol*. **2**, 1648–1657 (2017).

9. F. Cava, M. A. de Pedro, H. Lam, B. M. Davis, M. K. Waldor, Distinct pathways for modification of the bacterial cell wall by non-canonical D-amino acids. *The EMBO Journal*. **30**, 3442–3453 (2011).

10. A. N. Sanders, L. F. Wright, M. S. Pavelka, Genetic characterization of mycobacterial L,D-transpeptidases. *Microbiology (Reading, Engl.)*. **160**, 1795–1806 (2014).

11. J. E. Long *et al.*, in *Gene Essentiality* (Humana Press, New York, NY, New York, NY, 2015), vol. 1279 of *Gene Essentiality: Methods and Protocols*, pp. 79–95.

12. K. J. Kieser *et al.*, Phosphorylation of the Peptidoglycan Synthase PonA1 Governs the Rate of Polar Elongation in Mycobacteria. *PLoS Pathog*. **11**, e1005010 (2015).

13. L. Zimmermann *et al.*, A Completely Reimplemented MPI Bioinformatics Toolkit with a New HHpred Server at its Core. *J. Mol. Biol.* (2017), doi:10.1016/j.jmb.2017.12.007.

14. A. Bansal *et al.*, A putative low-molecular-mass penicillin-binding protein (PBP) of Mycobacterium smegmatis exhibits prominent physiological characteristics of DD-carboxypeptidase and beta-lactamase. *Microbiology (Reading, Engl.)*. **161**, 1081–1091 (2015).

15. S. M. González-Leiza, M. A. de Pedro, J. A. Ayala, AmpH, a bifunctional DD-endopeptidase and DD-carboxypeptidase of Escherichia coli. *Journal of Bacteriology*. **193**, 6887–6894 (2011).

16. J.-L. Mainardi *et al.*, Unexpected inhibition of peptidoglycan LD-transpeptidase from Enterococcus faecium by the beta-lactam imipenem. *Journal of Biological Chemistry*. **282**, 30414–30422 (2007).

17. K. M. Papp-Wallace, A. Endimiani, M. A. Taracila, R. A. Bonomo, Carbapenems: past, present, and future. *Antimicrobial Agents and Chemotherapy*. **55**, 4943–4960 (2011).

18. R. Gupta *et al.*, The Mycobacterium tuberculosis protein LdtMt2 is a nonclassical transpeptidase required for virulence and resistance to amoxicillin. *Nature Medicine*. **16**, 466–469 (2010).

19. X. Gonzalo, F. Drobniewski, Is there a place for β-lactams in the treatment of multidrug-resistant/extensively drug-resistant tuberculosis? Synergy between meropenem and amoxicillin/clavulanate. *J. Antimicrob. Chemother.* **68**, 366–369 (2013).

20. in *Clinical Microbiology Procedures Handbook, Fourth Edition* (American Society of Microbiology, 2016), pp. 5.16.1–5.16.23.

21. N. Andreu, T. Fletcher, N. Krishnan, S. Wiles, B. D. Robertson, Rapid measurement of antituberculosis drug activity in vitro and in macrophages using bioluminescence. *J. Antimicrob. Chemother.* **67**, 404–414 (2012).

22. T. S. Ursell *et al.*, Rod-like bacterial shape is maintained by feedback between cell curvature and cytoskeletal localization. *Proc. Natl. Acad. Sci. U.S.A.* **111**, E1025–34 (2014).

23. E. C. Garner *et al.*, Coupled, Circumferential Motions of the Cell Wall Synthesis Machinery and MreB Filaments in B. subtilis. *Science*. **333**, 222–225 (2011).

24. S. Hussain *et al.*, MreB filaments align along greatest principal membrane curvature to orient cell wall synthesis. *eLife*. **7**, e32471 (2018).

25. M. A. DeJesus, C. Ambadipudi, R. Baker, C. Sassetti, T. R. Ioerger, TRANSIT - A Software Tool for Himar1 TnSeq Analysis. *PLoS Comput Biol*. **11**, e1004401–17 (2015).

26. N. Andreu *et al.*, Optimisation of bioluminescent reporters for use with mycobacteria. *PLoS ONE*. **5**, e10777 (2010).

27. C. C. Boutte *et al.*, A cytoplasmic peptidoglycan amidase homologue controls mycobacterial cell wall synthesis. *eLife*. **5**, a021113 (2016).

28. D. G. Gibson *et al.*, Enzymatic assembly of DNA molecules up to several hundred kilobases. *Nature Methods*. **6**, 343–345 (2009).

29. K. C. Murphy, K. Papavinasasundaram, C. M. Sassetti, Mycobacterial recombineering. *Methods Mol. Biol.* **1285**, 177–199 (2015).

30. K. J. Kieser *et al.*, Peptidoglycan synthesis in Mycobacterium tuberculosis is organized into networks with varying drug susceptibility. *Proc. Natl. Acad. Sci. U.S.A.* **112**, 13087–13092 (2015).

31. E. Kuru, S. Tekkam, E. Hall, Y. V. Brun, M. S. Van Nieuwenhze, Synthesis of fluorescent D-amino acids and their use for probing peptidoglycan synthesis and bacterial growth in situ. *Nat Protoc*. **10**, 33–52 (2014).

32. E. H. Rego, R. E. Audette, E. J. Rubin, Deletion of a mycobacterial divisome factor collapses single-cell phenotypic heterogeneity. *Nature*. **546**, 153–157 (2017).

33. H. A. Eskandarian *et al.*, Division site selection linked to inherited cell surface wave troughs in mycobacteria. *Nat Microbiol*. **2**, 17094 (2017).

34. J. H. Koschwanez, R. H. Carlson, D. R. Meldrum, Thin PDMS films using long spin times or tert-butyl alcohol as a solvent. *PLoS ONE*. **4**, e4572 (2009).

35. A. L. Thangawng, R. S. Ruoff, M. A. Swartz, M. R. Glucksberg, An ultra-thin PDMS membrane as a bio/micro-nano interface: fabrication and characterization. *Biomed Microdevices*. **9**, 587–595 (2007).

36. N. Dhar, D. Bousbaine, Y. Wakamoto, J. D. McKinney, I. Santi, Single-cell dynamics of the chromosome replication and cell division cycles in mycobacteria. *Nature Communications*. **4**, 1–10 (2013).

37. J. Schindelin *et al.*, Fiji: an open-source platform for biological-image analysis. *Nature Methods*. **9**, 676–682 (2012).

38. A. Paintdakhi *et al.*, Oufti: an integrated software package for high-accuracy, high-throughput quantitative microscopy analysis. *Molecular Microbiology*. **99**, 767–777 (2016).

39. Y. Qiao *et al.*, Detection of lipid-linked peptidoglycan precursors by exploiting an unexpected transpeptidase reaction. *J. Am. Chem. Soc.* **136**, 14678–14681 (2014).

40. Y. Qiao *et al.*, Lipid II overproduction allows direct assay of transpeptidase inhibition by β-lactams. *Nature Chemical Biology*. **13**, 793–798 (2017).

41. Y. Rebets *et al.*, Moenomycin resistance mutations in Staphylococcus aureus reduce peptidoglycan chain length and cause aberrant cell division. *ACS Chem. Biol.* **9**, 459–467 (2014).

42. M. D. Lebar *et al.*, Reconstitution of peptidoglycan cross-linking leads to improved fluorescent probes of cell wall synthesis. *J. Am. Chem. Soc.* **136**, 10874–10877 (2014).

43. M. A. Welsh *et al.*, Identification of a Functionally Unique Family of Penicillin-Binding Proteins. *J. Am. Chem. Soc.* **139**, 17727–17730 (2017).

Acknowledgments:

We thank Cara Boutte for discussion and thorough manuscript review. We are grateful to the Rubin and Fortune laboratory for discussion and input. We also thank the Microbiology and Immunobiology department at Harvard Medical School for sharing equipment and reagents, as well as the BSL3 staff at the Harvard School of Public health for tremendous support. This work was supported by the National Institutes of Health U19 AI107774 to E.J.R and T.R.I., F32AI104287 to E.H.R (who is also supported by a Career Award at the Scientific Interface from BWF), R01 GM76710 to S.W., R01AI083365 and U19AI109764 to T.G.B.. M.A.W. is supported by an F32 GM123579. LT.S. was supported by an American Heart Association Postdoctoral fellowship (14POST18480014). H.C.L is funded by a Simons Foundation Fellow of the Life Sciences Research Foundation award. This work was also supported in part by the Swiss National Science Foundation (310030_156945) and the Innovative Medicines Initiative (115337) to J.D.M., and from the Swiss National Science Foundation (205321_134786 and 205320_152675), the European Union FP7/2007-2013/ERC Grant Agreement No. 307338 (NaMic), and EU-FP7/Eurostars E!8213 to G.E.F. Support for H.A.E. comes from a European Molecular Biology Organization Long Term Fellowships (191-2014 and 750-2016). K.J.K. was

supported by the National Science Foundation Graduate Research Fellowship (DGE1144152, DGE0946799).

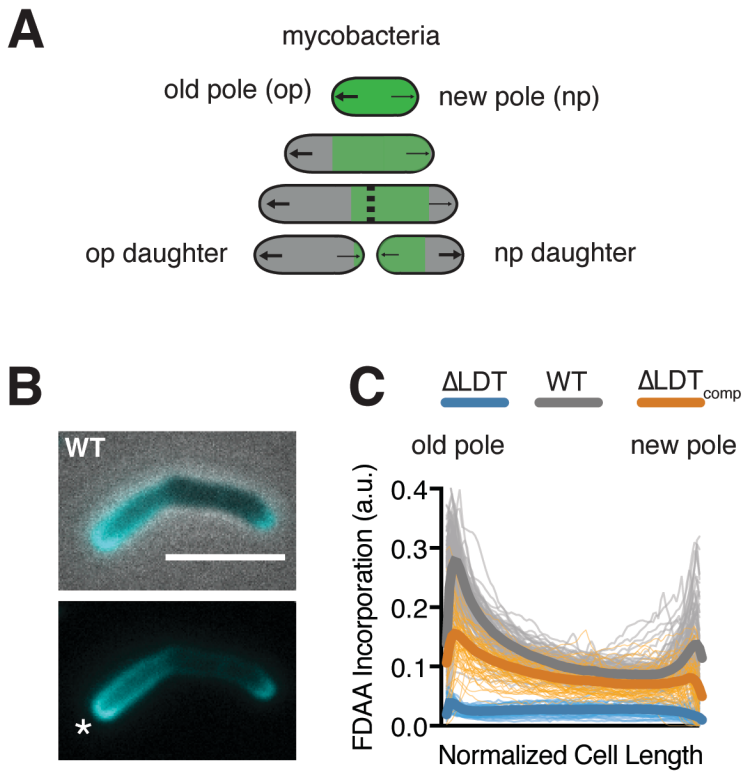

Figure 1: FDAAs are incorporated asymmetrically by LD-transpeptidases. (A) Schematic of mycobacterial asymmetric polar growth. Green, old cell wall; grey, new material; dotted line, septum; large arrows, old pole growth; small arrows, new pole growth. **(B)** FDAA incorporation in log-phase WT Msm cell after 2-minute incubation. Scale bar=5µm. Old pole marked with (*). **(C)** Profiles of FDAA incorporation in log-phase WT (N=98), ΔLDT (N=40), and ΔLDTcomp (N=77) cells. Thick lines represent mean incorporation profile, thin lines are FDAA incorporation in single cells.

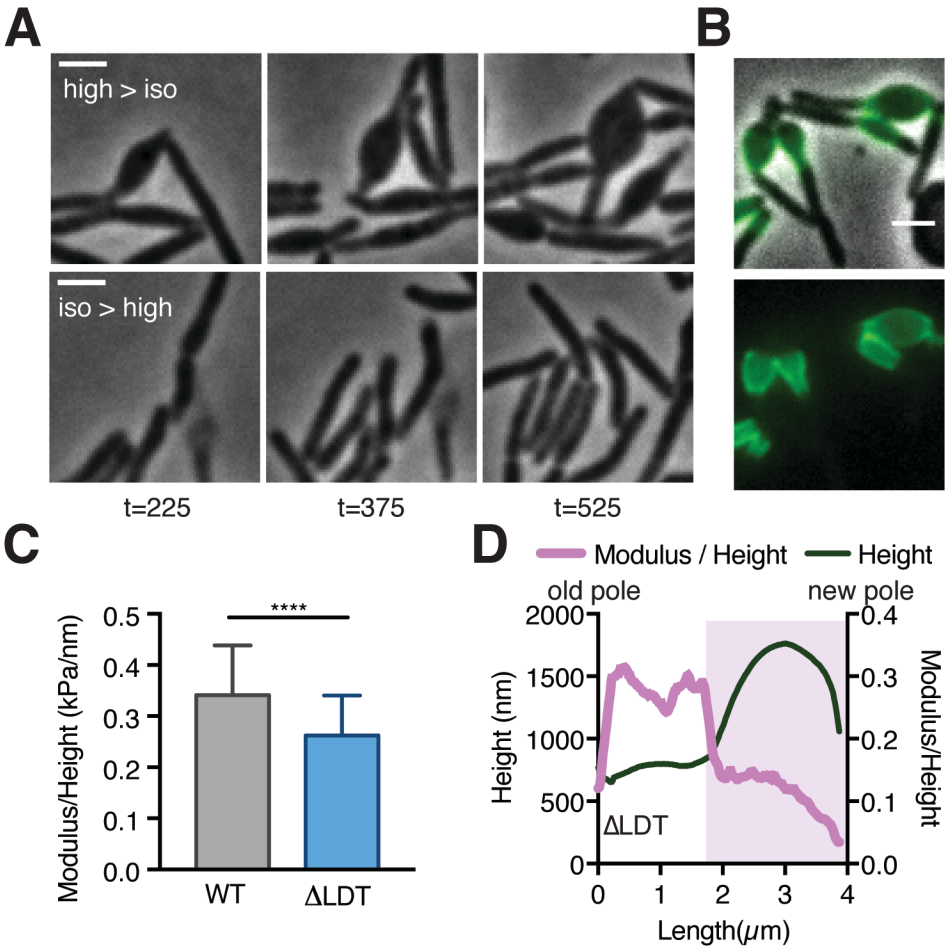

Figure 2: LDT catalyzed 3-3 crosslinks are required for rod shape maintenance at aging cell wall. (A) Msm ΔLDT time-lapse microscopy of cells switched from high- to iso- (top) osmolar media, or iso- to high osmolar media (bottom). (high=7H9+150mM sorbitol; iso=7H9). t= time in minutes post osmolarity switch. **(B)** ΔLDT cells were stained with Alexa 488 NHS-ester (green), washed, and visualized after outgrowth. A,B scale bar=2µm. **(C)** Mean stiffness of WT (N=73) and ΔLDT (N=47) Msm cells as measured by atomic force microscopy. Mann-Whitney U P-Value **** < 0.0001. (D) Representative profile of cell height and height-normalized stiffness (modulus/height) in a single ΔLDT cell. Pink shaded portion highlights location of a bleb.

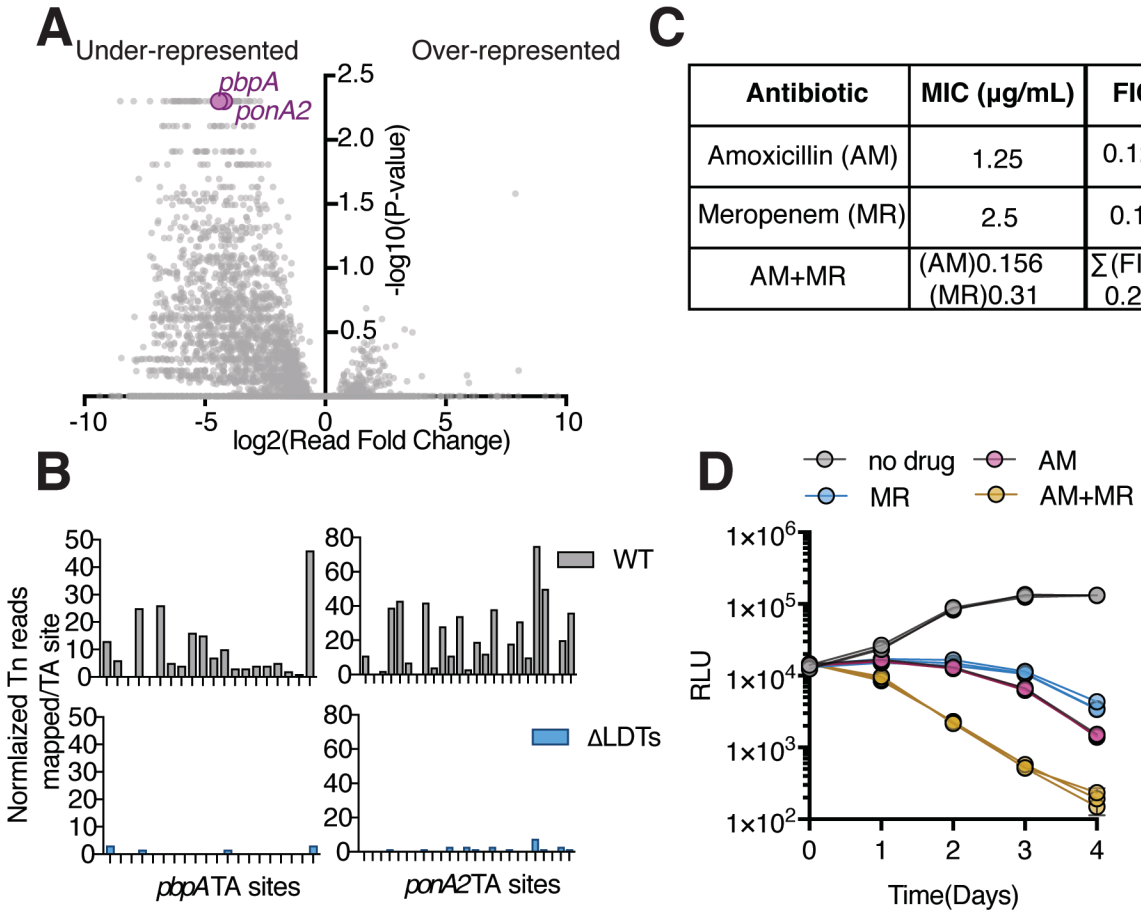

Antibiotic	MIC (µg/mL)	FIC
Amoxicillin (AM)	1.25	0.1248
Meropenem (MR)	2.5	0.124
AM+MR	(AM)0.156 (MR)0.31	∑(FICs)= 0.2488

Figure 3: Mycobacteria are hypersensitive to PBP inactivation in the absence of LDTs. (A) Fold change in the number of reads for transposon insertion counts in ΔLDT cells compared to WT Msm. P-value is derived from a rank sum test (*25*). **(B)** Transposon insertions per TA site in *pbpA* and *ponA2* in WT and ΔLDT cells. **(C)** Minimum inhibitory concentration (MIC) of amoxicillin, meropenem, or the combination, in *M. tuberculosis*. FIC (fractional inhibitory concentration) = MIC of drug in combination/MIC of drug alone. Synergy is defined as ∑FIC<=0.5. **(D)** Killing dynamics of *M. tuberculosis* (expressing the *luxABCDE* operon from Photorhabdus luminescens(*26*)) measured via luciferase production (RLU=relative light units). 5X MIC Amoxicillin (AM) (3.125 µg/mL); 5X MIC Meropenem (MR) (6.25 µg/mL); Amoxicillin+Meropenem 3.125 µg/mL AM; 6.25 µg/mL MR) . Biological triplicate are plotted. All drugs were used in combination with 5µg/mL clavulanate.

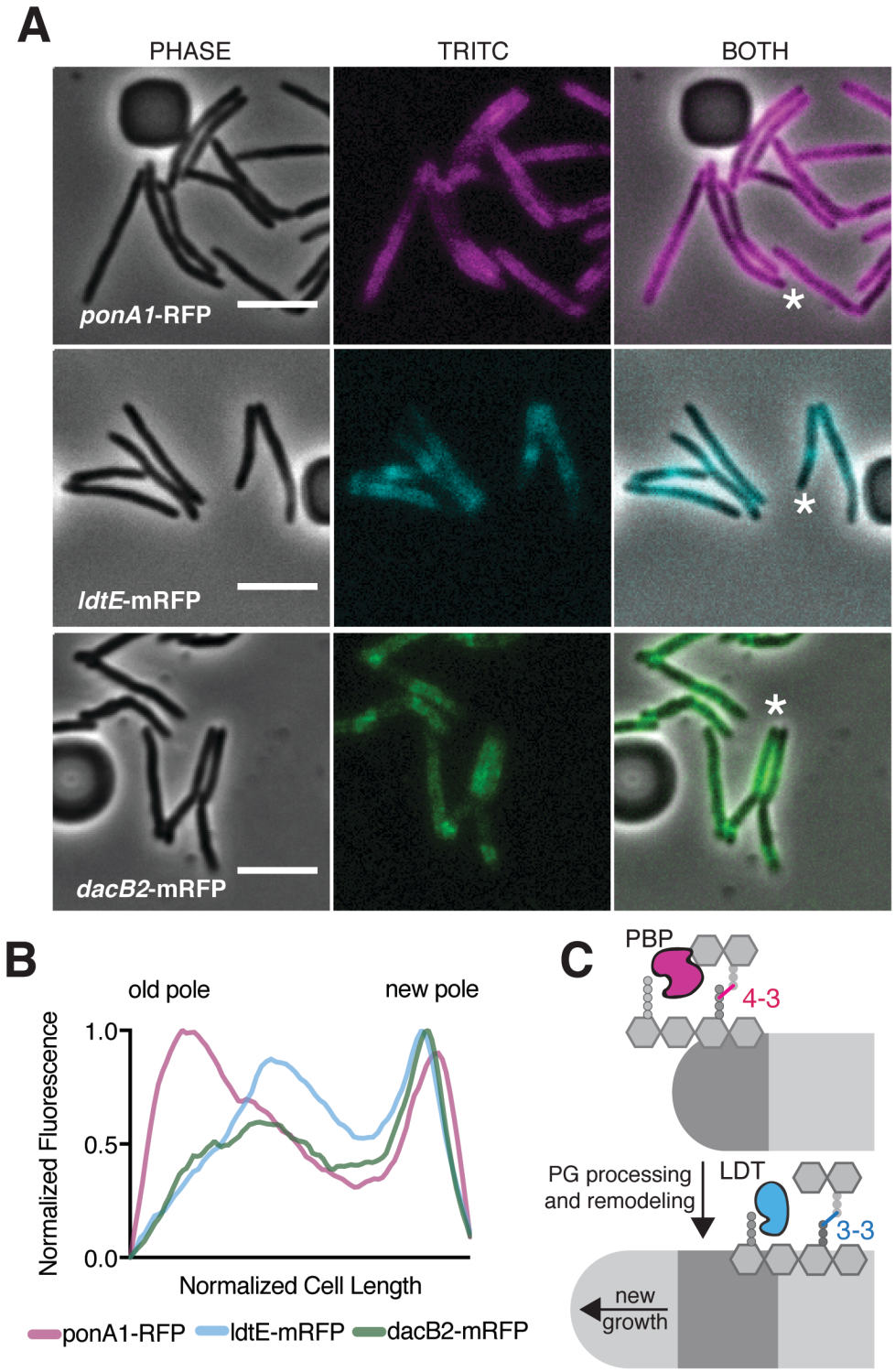

Figure 4: Peptidoglycan synthesizing enzymes localize to differentially aged cell wall. (A) Representative fluorescence images of PonA1-RFP (magenta), LdtE-mRFP (cyan), and DacB2-mRFP (green). Scale bars=5µm. **(B)** Average PonA1-RFP (N=24), LdtE-mRFP (N=23) or DacB2-mRFP (N=23) distribution in cells before division. **(C)** A model for PG age and crosslink segregation via polar growth in mycobacteria

Supplementary Materials for

Maturing Mycobacterial Peptidoglycan Required Non-canonical Crosslinks to Maintain Shape

Catherine Baranowski[1], Lok-To Sham[2,3], Haig A. Eskandarian[4,5], Michael A. Welsh[2], Hoong C. Lim[2], Karen J. Kieser[1], Jeffrey C. Wagner[1], Suzanne Walker[2], John D. McKinney[4], Georg E. Fantner[5], Thomas R. Ioerger[6], Thomas G. Bernhardt[2], Eric J. Rubin[1,2]*, E. Hesper Rego[7*]

Materials and Methods

Bacterial strains and culture conditions

Unless otherwise stated, all *Mycobacterium smegmatis* (mc^2155) was grown shaking at 37°C in liquid 7H9 media consisting of Middlebrook 7H9 salts with 0.2% glycerol, 0.85g/L NaCl, ADC (5g/L albumin, 2g/L dextrose, 0.003g/L catalase), and 0.05% Tween 80 and plated on LB agar. *Mycobacterium tuberculosis* (H37Rv) was grown in liquid 7H9 with OADC (oleic acid, albumin, dextrose, catalase) with 0.2% glycerol and 0.05% Tween 80. Antibiotic selection for *M. smegmatis* and *M. tuberculosis* were done at the following concentrations in broth and on agar: 25μg/mL kanamycin, 50μg/mL hygromycin, 20μg/mL zeocin and 20μg/mL nourseothricin and, twice those concentrations for cloning in *Escherichia coli* (TOP10, XL1-Blue and DH5α).

Strain construction

M. smegmatis mc^2155 mutants lacking *ldtABECFG (*ΔLDT) was constructed using recombineering to replace endogenous copies with zeocin or hygromycin resistance cassettes flanked by lox sites as previously described (*27*). Briefly, 500 base pairs of upstream and downstream sequence surrounding the gene of interest were amplified via PCR (KOD Xtreme™ Hot Start DNA polymerase (EMD Millipore, Billerica, MA)). These flanking regions were amplified with overlaps to either a zeocin or hygromycin resistance cassette flanked by loxP sites and these pieces were assembled into a knock-out construct via isothermal assembly (*28*). Each knock-out cassette was transformed into Msm expressing inducible copies of RecET for recombination (*29*). Once knock-outs were verified by PCR using and sequencing, the antibiotic resistance cassettes were removed by the expression of Cre recombinase. The order of knock-out construction in the ΔLDT strain was as follows (where arrows represent

transformation of a Cre-recombinase plasmid, followed by curing of the Cre-recombinase plasmid as it contains the *sacB* gene for sucrose counter selection on LB supplemented with 10% sucrose, and strain names are listed in parenthesis). This resulted in the removal of antibiotic cassettes flanked by loxP sites:

1) mc^{2}155Δ*ldtA*:: zeo^R (KB103)→ mc^{2}155Δ*ldtA*::loxP (KB134)

2) mc^{2}155Δ*ldtA::loxP* + Δ*ldtE*:: zeo^R (KB156)

3) mc^{2}155Δ*ldtA::loxP* Δ*ldtE*:: zeo^R + Δ*ldtB*:: hyg^R (KB200) → mc^{2}155Δ*ldtA::loxP* Δ*ldtE*::loxP Δ*ldtB*::loxP (KB207)

4) mc^{2}155Δ*ldtA::loxP* Δ*ldtE*::loxP Δ*ldtB*::loxP + Δ*ldtC*:: hyg^R (KB209)

5)mc^{2}155Δ*ldtA::loxP* Δ*ldtE*::loxP Δ*ldtB*::loxP Δ*ldtC*:: hyg^R Δ*ldtG*:: zeo^R (KB222)→ mc^{2}155Δ*ldtA::*loxP Δ*ldtE*::loxP Δ*ldtB*::loxP Δ*ldtC*:: loxP Δ*ldtG*:: loxP (KB241)

6) mc^{2}155Δ*ldtA::*loxP Δ*ldtE*::loxP Δ*ldtB*::loxP Δ*ldtC*:: loxP Δ*ldtG*:: loxP Δ*ldtF*:: hyg^R (KB303 referred to as ΔLDT) .

M. tuberculosis H37Rv was transformed with a vector expressing the codon optimized *Photorhabdus luminescens luxABCDE* operon (pMV306hsp+LuxG13 –Addgene #26161)(*26*). This strain is referred to as Mtb Lux.

Refer to Supplemental Table 1 for oligonucleotides, and Supplemental Table 2 for a complete strain list.

<u>ΔLDT complementation plasmid construction</u>

To complement ΔLDT we placed a copy of *ldtE* (*MSMEG_0233*) under the constitutive TetO promoter (a UV15 derivative within a pMC1s plasmid that is inducible with anhydrous tetracycline in the presence of a tet-repressor TetR, which the ΔLDT_{comp} strain lacks (*12*)) on vector that integrates at the L5 phage integration site of the chromosome of the ΔLDT strain (the vector is marked with kanamycin resistance). A glycine, glycine, serine linker was cloned between *ldtE* and mRFP in this complementation construct.

PonA1 transpeptidase essentiality L5 allele swapping

To test essentiality of transpeptidation by PonA1 in the ΔLDT cells, L5 allele swapping as described in (*12*) and figure S9 was performed. The plasmids used in this experiment were previously published in (*12*). Briefly, a wild-type copy of PonA1 (TetO driven expression, L5 integrating and kanamycin marked) was transformed into ΔLDT. Then, the endogenous copy of *ponA1* was replaced with zeocin using the above mentioned recombineering technique (amplifying the construct from a previously published knockout of *ponA1*(*12*)). Swapping efficiency of either wildtype or transpeptidase mutant PonA1 marked with nourseothricin was tested with a transformation into ΔLDT//L5-TetO-ponA1 (WT)-kanamycin.

M. tuberculosis minimum inhibitory concentration (MIC) determination

Mtb Lux was grown to log phase and diluted to an OD_{600}=0.006 in each well of non-treated 96 well plates (Genessee Scientific) containing 100µL of meropenem (Sigma Aldrich) and/or amoxicillin (Sigma Aldrich) diluted in 7H9+OADC+5µg/mL clavulanate (Sigma Aldrich). Cells were incubated in drug at 37°C shaking for 7 days, 0.002% resazurin (Sigma Aldrich) was added to each well, and the plates were incubated for 24 hours before MICs were determined. Pink

wells signify metabolic activity and blue signify no metabolic activity. (*30*) Checkerboard MIC plates and fractional inhibitory concentrations were calculated as described in (*20*).

M. tuberculosis drug killing assays

Mtb Lux was grown to log phase (kanamycin 25µg/mL) and diluted in 30mL inkwells (Corning Lifesciences) to an OD_{600}=0.05 in 7H9+OADC+5µg/mL clavulanate with varying concentrations of amoxicillin, meropenem, or both. 100µL of these cultures were pipetted in duplicate into a white 96-well polystyrene plate (Greiner Bio-One) and luminescence was read in a Synergy H1 microplate reader from BioTek Instrumenmts, Inc. using the Gen5 Software (2.02.11 Installation version). The correlation between relative light units (RLU) and colony forming units (CFU) is shown in Msm in supplemental figure S9.

Fluorescent D-amino acid labeling

NADA (3-[7-nitrobenzofurazan]-carboxamide-D-alanine), HADA (3-[7-hydroxycoumarin]-carboxamide-D-alanine) and TADA (3-[5-carboxytetramethylrhodamine]-carboxamide-D-alanine) were synthesized by Tocris following the published procotol (*31*). To 1mL of exponentially growing cells 0.1mM of FDAA final was added and incubated for 2 minutes before washing in 7H9 twice. For still imaging, after the second wash, cells were fixed in 7H9 + 1% paraformaldehyde before imaging. For pulse chase experiments, cells were stained, washed with 7H9 and allowed to grow out for 40 minutes before being stained with a second dye and imaged.

Flow cytometry

An *M. smegmatis* transposon library was grown to mid-log phase, and stained with 2 µg/mL NADA for 2 minutes. Cells were centrifuged and half of the supernatant was discarded. The pellet was resuspended in the remaining supernatant, passed through a 10µm filter and taken to be sorted (FACSAria; Excitation: 488nm; Emission filter: 530/30). Two bins were drawn at the lowest and highest staining end of the population, representing 12.5% of the population. 600,000 cells from these bins were sorted into 7H9 medium. Half of this was directly plated onto LB agar supplemented with kanamycin to select for cells harboring the transposon. The remaining 300,000 cells were grown out in 7H9 to log phase, stained with FDAA and sorted again to enrich the populations.

Transposon sequencing, mapping and FDAA flow cytometry enrichment analysis.

Genomic DNA (gDNA) was harvested from the sorted transposon library colonies and transposon-gDNA junction libraries were constructed and sequenced using the Illumina Hi-Seq platform (*11*). Reads were mapped on the *M. smegmatis* genome, tallied and reads at each TA site for the bins (low/high incorporating sort 1 and 2) were imported into MATLAB and processed by a custom scripts as described in(*32*).

Microscopy

Both still imaging and time lapse microscopy were performed on an inverted Nikon TI-E microscope at 60x magnification. Time lapse was done using a CellASIC (B04A plate) with constant liquid 7H9 flow in a 37°C chamber. For turgor experiment (Figure 3.4A), cells were grown in either 7H9 or 7H9 500mM sorbitol overnight, and then switched to either 7H9 with 150mM sorbitol (high osmolar) or to 7H9 alone (iso-osmolar).

Atomic force microscopy

AFM experimentation was conducted as previously(*33*). In short, polydimethylsiloxane (PDMS) – coated coverslips were prepared by spin-coating a mixture of PDMS at a ratio of 15:1 (elastomer:curing agent) with hexane (Sigma 296090) at a ratio of 1:10 (PDMS:hexane) (*34*, *35*). A 50 µl filtered (0.5 µm pore size PVDF filter – Millipore) aliquot of bacteria grown to mid-exponential phase and concentrated from 2-5 ml of culture was deposited onto the hydrophobic surface of a PDMS-coated coverslip and incubated for ~20 min to increase surface interactions between bacteria and the coverslip. 7H9 medium (~3 ml) was supplied to the sample so as to immerse the bacterial sample and the AFM cantilever in fluid. The AFM imaging mode, Peak Force QNM, was used to image bacteria with a Nanoscope 5 controller (Veeco Metrology) at a scan rate of 0.5 Hz and a maximum Z-range of 12 µm. A ScanAsyst fluid cantilever (Bruker) was used. Height, peak force error, DMT modulus, and log DMT modulus were recorded for all scanned images in the trace and retrace directions. Images were processed using Gwyddion (Department of Nanometrology, Czech Metrology Institute). ImageJ was used for extracting bacterial cell profiles in a tabular form.

Correlated optical fluorescence and AFM

Correlated optical fluorescence and AFM images were acquired as described(*33*). Briefly, optical fluorescence images were acquired with an electron-multiplying charge-coupled device (EMCCD) iXon Ultra 897 camera (Andor) mounted on an IX81 inverted optical microscope (Olympus) equipped with an UPLFLN100XO2PH x100 oil immersion objective (Olympus). Transmitted light illumination was provided by a 12V/100W AHS-LAMP halogen lamp. An U-

MGFPHQ fluorescence filter cube for GFP with HQ-Ion-coated filters was used to detect GFP fluorescence. The AFM was mounted on top of the inverted microscope, and images were acquired with a Dimension Icon scan head (Bruker) using ScanAsyst fluid cantilevers (Bruker) with a nominal spring constant of 0.7 N m^{-1} in Peak Force QNM mode at a force setpoint ~1nN and typical scan rates of 0.5 Hz. Indentation on the cell surface was estimated to be ~10 nm in the Z-axis. Optical fluorescence microscopy was used to identify Wag31-GFP puncta expressed in a wild-type background(*36*) in order to distinguish them from cells of the ΔLDT mutant strains.

Calculating cell surface rigidity

A cell profile was extracted from AFM Height and DMT Modulus image channels as sequentially connected linear segments following the midline of an individual cell. A background correction was conducted to by dividing the DMT modulus values of the cell surface by the mean value of the PDMS surface and rescaled to compare the cell surface rigidity between individual cells from different experiments. The DMT modulus reflects the elastic modulus (stress-strain relationship) for each cross-sectional increment along the cell length.

Analysis of fluorescent protein distribution

Using a segmented line, profiles of cells from new to old pole were created at the frame "pre-division" based on physical cell separation of the phase image. A custom FIJI (*37*) script was run to extract fluorescence line profiles of each cell and save them as .csv files. These .csv files were imported to Matlab where a custom script was applied to normalize the

fluorescence line profile to fractional cell length and to interpolate the fluorescence values to allow for averaging.

Analysis of cell wall distribution

Cells were stained with Alexa488 NHS ester as described previously (*7*) and followed via time-lapse microscopy in the CellASIC device. Briefly, 1mL of log phase cells was pelleted at 8,000 rpm for 1 minute and washed with 1mL PBST. The pellet was resuspended in 100uL of PBST and 10uL Alexa Fluor 488 carboxylic acid succinimidyl ester was added for a final concentration of 0.05mg/mL. This was incubated for 3 minutes at room temperature. Stained cells were pelleted for 1 minute at 13,000 rpm and washed with 500µL PBST. They were spun again and resuspended in 7H9 for outgrowth observation over time in the CellASIC device.

Analysis of FDAAs

Images were analyzed using a combination of Oufti(*38*) for cell selection followed by custom coded Matlab scripts to plot FDAA fluorescence over normalized cell length, calculate cell length and bin cells by existence of an FDAA labeled septum.

Generation of transposon libraries

M.smegmatis cells were transduced at (OD_{600} 1.1-1.7) with *φ*MycoMarT7 phage (temperature sensitive) that has a Kanamycin marked Mariner transposon as previously described (*11*). Briefly, mutagenized cells were plated at 37°C on LB plates supplemented with Kanamycin to select for phage transduced cells. Roughly 100,000 colonies per library were scraped, and genomic DNA was extracted. Sequencing libraries were generated specifically containing

transposon disrupted DNA. Libraries were sequenced on the Illumina platform. Data were analyzed using the TRANSIT pipeline (*25*).

Peptidoglycan isolation and analysis

600mLs of wildtype and ΔLDT cells were grown to log phase and collected via centrifugation at 5000 x g for 10 minutes at 4°C. The resulting pellet was resuspsended in PBS and cells were lysed using a cell disruptor at 35,000psi twice. Lysed cells were boiled in 10% SDS (sodium dodecyl sulfate) for 30 minutes and peptidoglycan was collected via centrifugation at 17,000 x g. Pellets were washed with 0.01% DDM(*n*-Dodecyl β-D-maltoside) to remove SDS and resuspended in 1XPBS + 0.01% DDM. PG was digested with alpha amylase (Sigma A-6380) and alpha chymotrypsin (Amersco 0164) overnight. The samples were again boiled in 10% SDS and washed in 0.01% DDM. The resulting pellet was resuspended in 400µL 25mM sodium phosphate pH6, 0.5mM MgCl2, 0.01% DDM. 20µL of lysozyme (10mg/mL) and 20µL 5U/µL mutanolysoin (Sigma M9901) were added and incubated overnight at 37°C. Samples were heated at 100°C and centrifuged at 100,000 x g. 128µL of ammonium hydroxide was added and incubated for 5 hours at 37°C. This reaction was neutralized with 122µL of glacial acetic acid. Samples were lyophilized, resuspended in 300µL 0.1% formic acid and subjected to analysis by LC-MS/MS. Peptide fragments were separated with an Agilent Technologies 1200 series HPLC on a Nucleosil C18 column (5µm 100A 4.6 x 250mm) at 0.5mL/min flow rate with the following method: Buffer A= 0.1% Formic Acid; Buffer B=0.1% Formic Acid in acetonitrile; 0% B from 0-10 minutes, 0-20% B from 10-100 minutes, 20% B from 100-120 minutes, 20-80% B from 120-130 minutes, 80% B from 130-140 minutes, 80%-0% B from 140- 150minutes, 0% B from

150-170 minutes. MS/MS was conducted in positive ion mode using electrospray ionization on an Agilent Q-TOF (6520).

Expression and purification of MSMEG_2433 (DacB2)

MSMEG_2433 was expressed and purified using a modified method for purification of low molecular weight PBPs that was previously published (*39*). An N-terminally truncated MSMEG_2433$_{(29\text{-}296)}$ was cloned into the pET28b vector for isopropyl β-D-1-thiogalactopyranoside (IPTG) inducible expression in *E. coli* BL21 (DE3). 10mLs of overnight culture grown in LB with Kanamycin (50μg/mL) were diluted 1:100 into 1 L of LB with Kanamycin (50μg/mL) and grown at 37°C until an OD_{600} of 0.5. The culture was cooled to room temperature, induced with 0.5mM IPTG, and shaken at 16°C overnight. Cells were pelleted via centrifugation at 4,000rpm for 20 min at 4°C. The pellet was suspended in 20mL binding buffer (20mM Tris pH 8, 10mM $MgCl_2$, 160mM NaCl, 20mM imidazole) with 1mM phenylmethylsulfonylfluoride (PMSF) and 500μg/mL DNase. Cells were lysed via three passage through a cell disrupter at ≥ 10,000 psi. Lysate was pelleted by ultracentrifugation (90,000 × g, 30 min, 4°C). To the supernatant, 1.0mL washed Ni-NTA resin (Qiagen) was added and the mixture rocked at 4°C for 40 min. After loading onto a gravity column, the resin was washed twice with 10mL wash buffer (20mM Tris pH 8, 500mM NaCl, 20mM imidazole, 0.1% Triton X-100). The protein was eluted in 10mL of elution buffer (20 mM Tris pH8, 150mM NaCl, 300mM imidazole, 0.1% reduced Triton X-100) and was concentrated to 1 mL with a 10kD MWCO Amicon Ultra Centrifuge Filter. The final protein concentration was measured by reading absorbance at 280 nm and using the estimated extinction coefficient (29459 $M^{-1}cm^{-1}$) calculate concentration. The protein was diluted to 200μM in elution buffer with 10% glycerol, aliquoted, and stored at -80°C.

Proper folding of purified MSMEG_2433$_{(29-296)}$ was tested via Bocillin-FL binding. Briefly, 20μM of purified protein was added to penicillin G (100, 1000 U/mL in 20mM K_2HPO_4, 140mM NaCl, pH7.5) in a 9μL reaction. The reaction was incubated at 37°C for 1hour. 10μM Bocillin-FL was added and incubated at 37°C for 30 minutes. SDS loading dye was added the quench the reaction and samples were loaded onto a 4-20% gel. MSMEG_2433$_{(29-296)}$ bound by Bocillin-FL was imaged using a Typhoon 9400 Variable Mode Imager (GE Healthcare) (Alexa Excitation-488nm Emission-526nm).

Lipid II extraction.

B. subtilis Lipid II was extracted as previously published (*40*).

SgtB purification.

S. aureus SgtB was purified as previously published (*41*).

Purification of *B. subtilis* PBP1.

Purification of *B. subtilis* PBP1 was carried out as previously described (*42*).

In vitro Lipid II polymerization and crosslinking.

20 μM purified BS Lipid II was incubated in reaction buffer (50 mM HEPES pH 7.5, 10 mM $CaCl_2$) with either 5 μM PBP1 or 0.33 μM SgtB for 1 hour at room temperature. The enzymes were heat denatured at 95°C for 5 minutes. Purified MSMEG_2433$_{(29-296)}$ was added (20 uM, final) and the reaction was incubated at room temperature for 1 hour. Mutanolysin (1 μL of a 4000 U/mL stock) was added and incubated for 1.5 hours at 37 °C (twice). The resulting

muropeptides were reduced with 30 μL of $NaBH_4$ (10 mg/mL) for 20 minutes at room temperature with tube flicking every 5 minutes to mix. The pH was adjusted to ~4 using with 20% H_3PO_4 and the resulting product was lyophilized to dryness. The residue was resuspended in 18μL of water and analyzed via LC-MS as previously reported (*43*).

Fig. S1

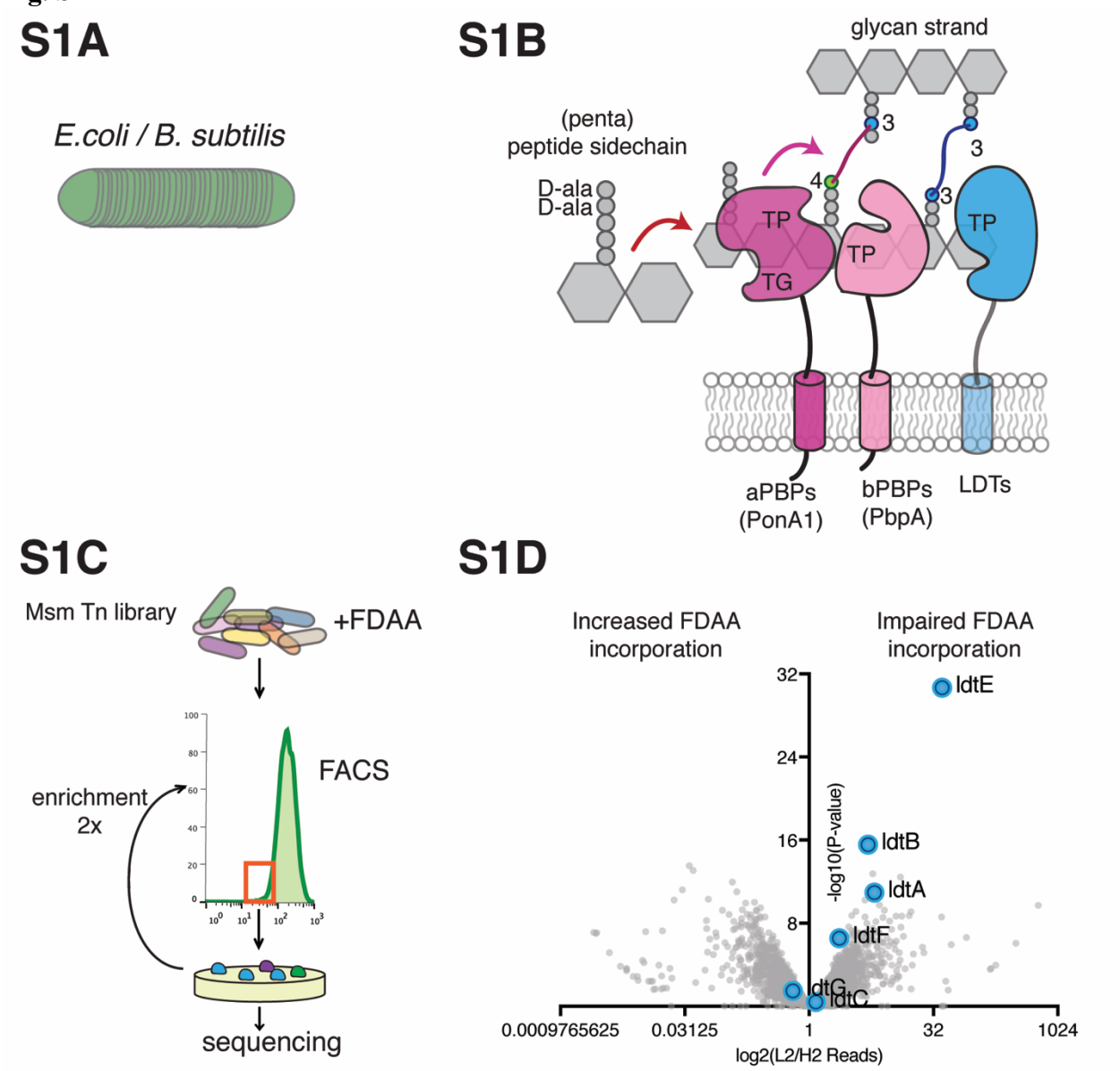

Figure S1: Peptidoglycan synthesis and FDAA screen overview. (A) *Escherchia coli* lateral cell wall growth. Unlike mycobacteria, *E. coli* inserts new cell wall along the lateral cell body, mixing old and new peptidoglycan. Green portion represents old cell wall, grey portion represents new material. **(B)** Cartoon of penicillin binding proteins (PBPs), L,D-transpeptidases (LDTs), and both 4-3 and 3-3 crosslinking. PBPs utilize a pentapeptide substrate found on new peptidoglycan, ending in D-alanine-D-alanine. LDTs utilize a tetrapeptide substrate found on processed peptidoglycan. TP, transpeptidase; TG, transglycosylase **(C)** Schematic of (Fluorescence Activated Cell Sorting (FACS)-based FDAA transposon library enrichment. A *Mycobacterium smegmatis* transposon library was stained with FDAAs, and the dimmest cells were sorted, grown, sorted again to enrich for transposon mutants that are unable to incorporate FDAA. **(D)** Results from S1C screen. Ratio (log2) of transposon reads per gene in the second sort low FDAA staining (L2) over the second sort high FDAA staining (H2) compared to the Mann-Whitney *U* P-value.

Fig. S2

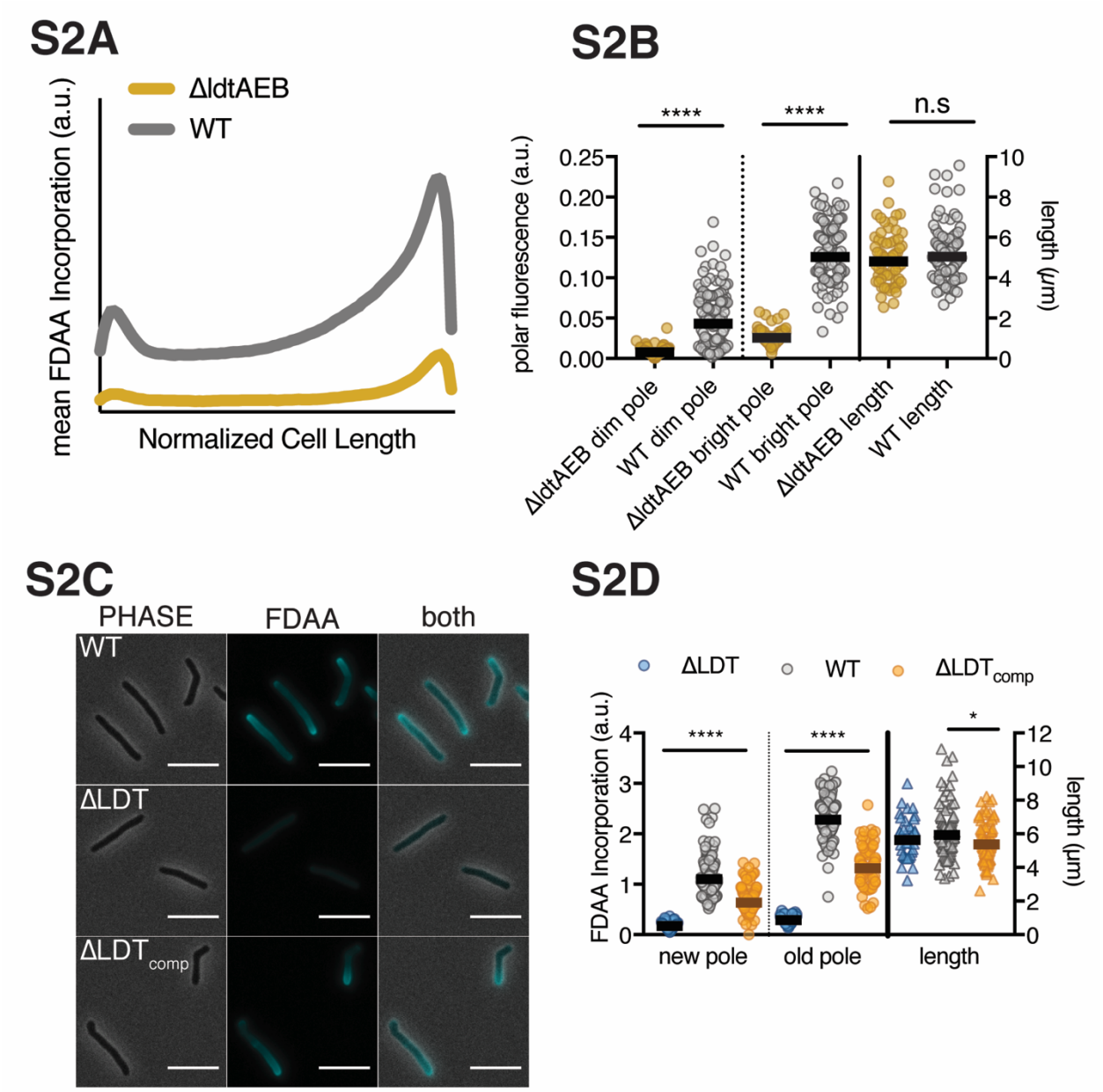

Figure S2: Fluorescent D-amino acid screen validation. (A) Mean line profiles (from new to old pole) of FDAA incorporation in log-phase WT (N=97), Δ*ldtABE* (N=64). **(B)** Quantification of FDAA incorporation at cell poles and quantification of cell length. Mann-Whitney U P-Value shown (**** P-Value < 0.0001). **(C)** Representative image of FDAA incorporation in log-phase WT, ΔLDT and ΔLDT_{comp} cells. Scale bar= 5μm. **(D)** Quantification of FDAA incorporation at poles and cell lengths of WT, ΔLDT and ΔLDT_{comp} cells shown in S2C and whose mean incorporation is shown in Figure 3C.

Fig. S3

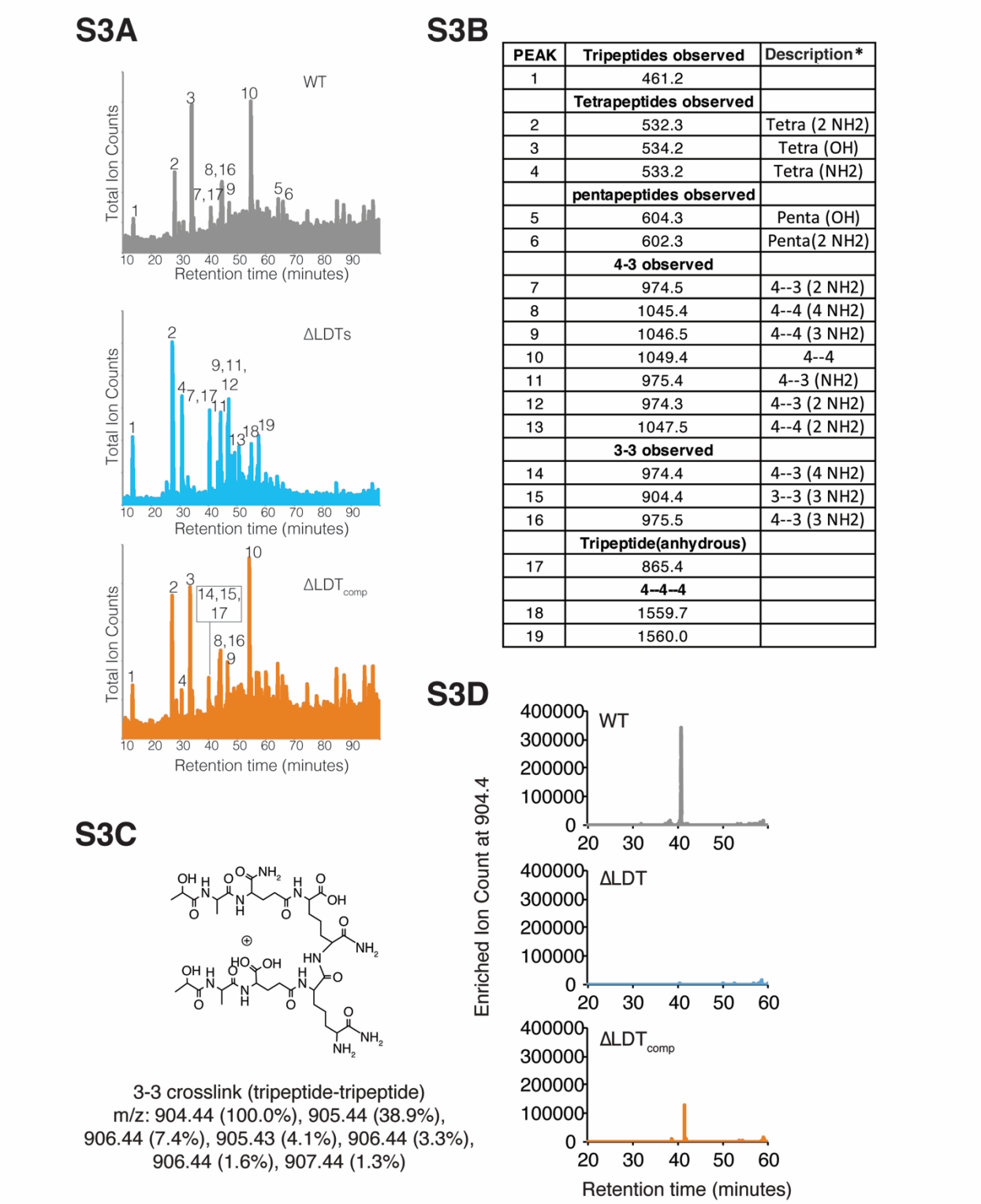

PEAK	Tripeptides observed	Description*
1	461.2	
	Tetrapeptides observed	
2	532.3	Tetra (2 NH2)
3	534.2	Tetra (OH)
4	533.2	Tetra (NH2)
	pentapeptides observed	
5	604.3	Penta (OH)
6	602.3	Penta(2 NH2)
	4-3 observed	
7	974.5	4--3 (2 NH2)
8	1045.4	4--4 (4 NH2)
9	1046.5	4--4 (3 NH2)
10	1049.4	4--4
11	975.4	4--3 (NH2)
12	974.3	4--3 (2 NH2)
13	1047.5	4--4 (2 NH2)
	3-3 observed	
14	974.4	4--3 (4 NH2)
15	904.4	3--3 (3 NH2)
16	975.5	4--3 (3 NH2)
	Tripeptide(anhydrous)	
17	865.4	
	4--4--4	
18	1559.7	
19	1560.0	

Figure S3: 3-3 crosslinks are not detectable in ΔLDT cells. (A) Total ion chromatograms of WT, ΔLDT and ΔLDT_{comp} peptidoglycan. **(B)** Table of muropeptide masses (Da) observed in

(S3A). The molecular weight difference by one of the identified peptides is due to differential amidation. The descriptions include the peptide lengths in the crosslink (4= tetra-, 3= tri- peptide) and the following parenthesis specifies the number of amidation in the species according to mass. **(C)** Structure of a representative 3-3 crosslink with a m/z=904.4. **(D)** Extracted ion chromatograms from WT, ΔLDT and ΔLDT_{comp} for a representative 3-3 crosslink with a m/z=904.4.

Fig. S4

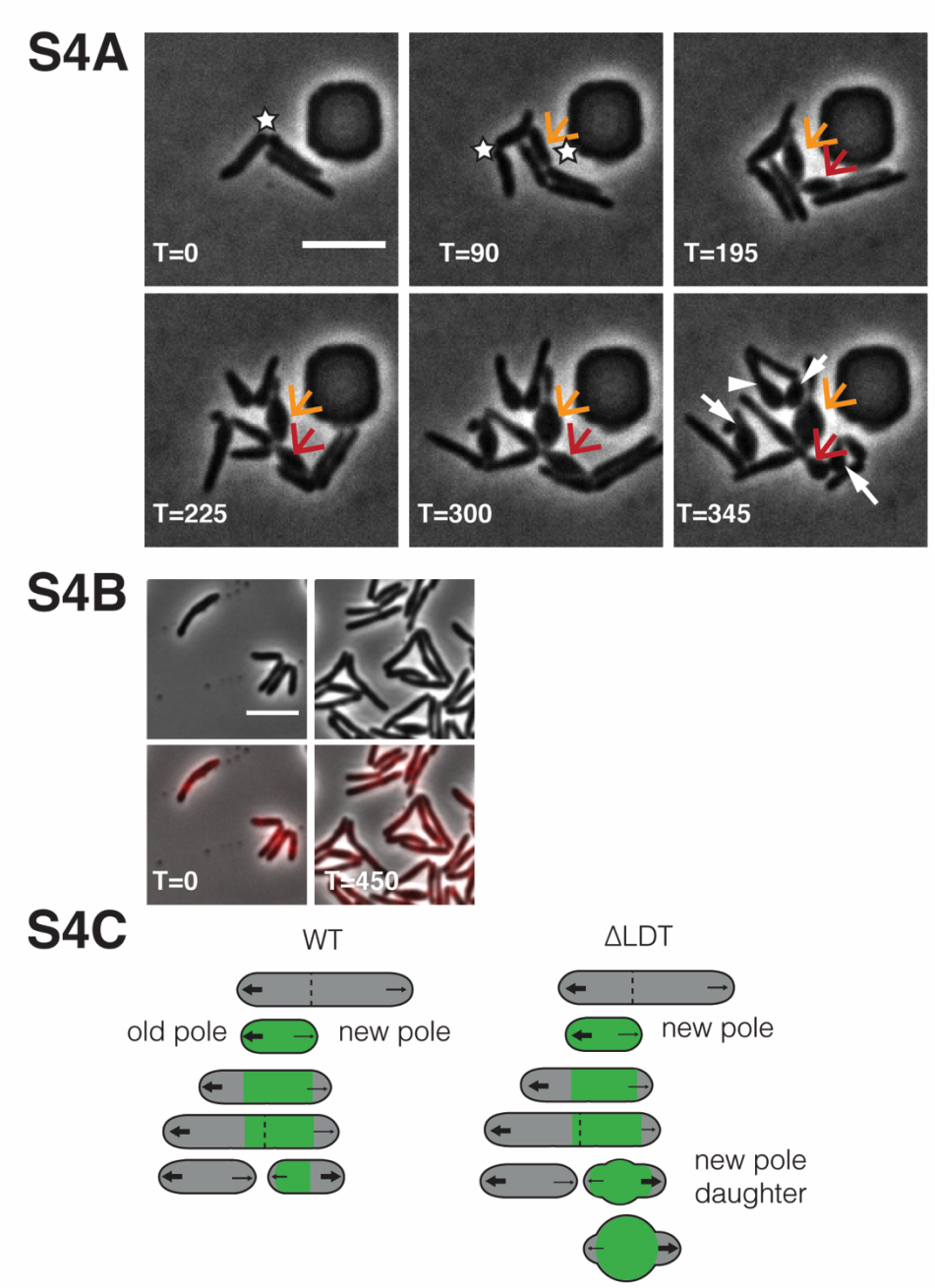

Figure S4: ΔLDT cell morphological characteristics. (A) Time-lapse microscopy montage of ΔLDT cells. The white stars mark new poles. The orange arrow points to the first new pole daughter cell of this series. The red arrow indicates the second resulting new pole daughter cell. In the last frame, white arrows point to all new pole daughter cells (besides the orange arrow and red arrow). **(B)** Time-lapse microscopy of ΔLDT_{comp} cells expressing LdtE-mRFP. **(C)** Model of rod-shape loss in old cell wall of ΔLDT cells compared to WT. Green portions of the cell represents old cell wall, grey portion represents new cell wall. The larger arrows indicate more growth from the old pole, while smaller arrows show less relative growth from the new pole. Dotted lines represent septa. All scale bars=5μm

Fig. S5

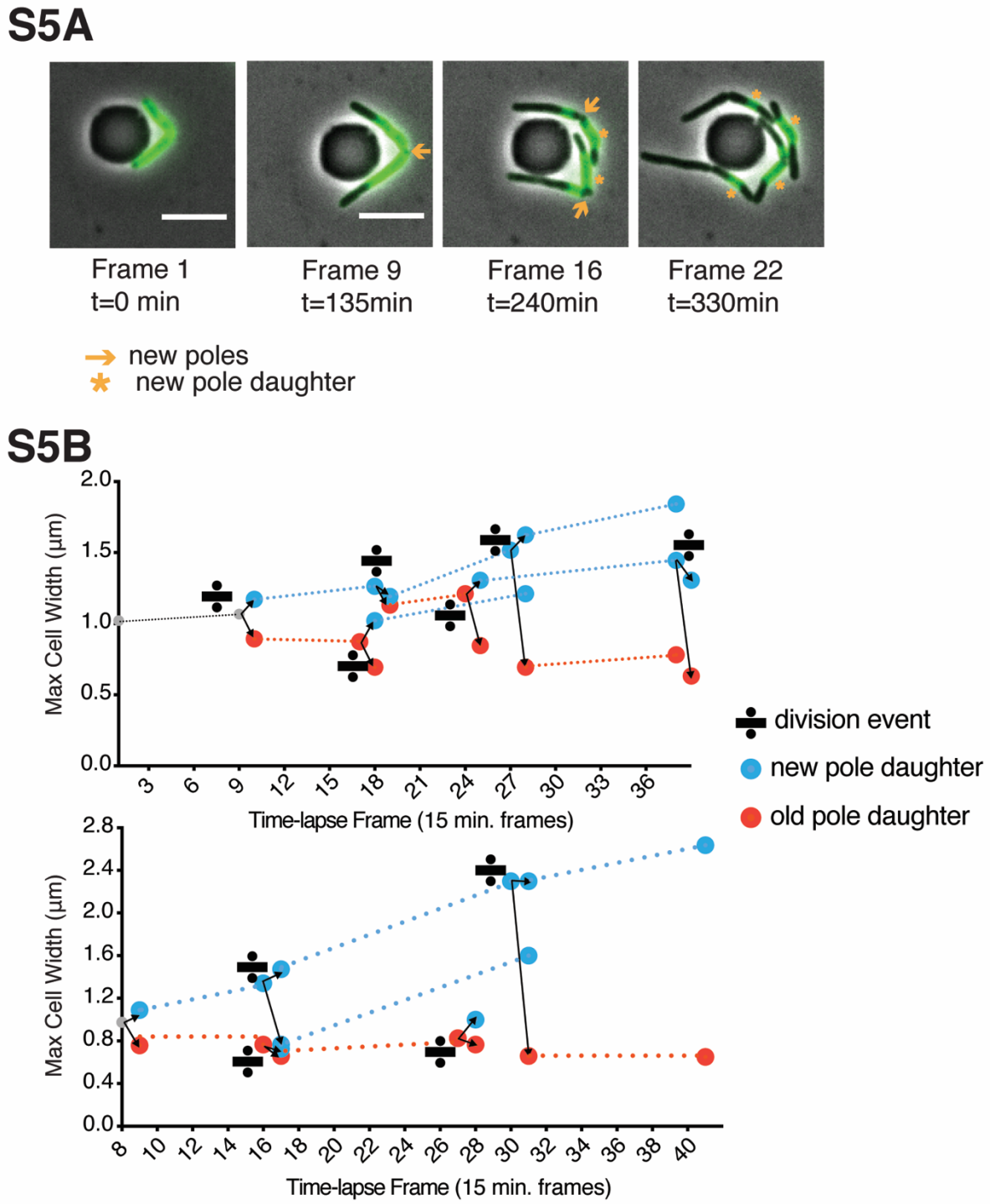

Figure S5: Inheritance of old cell wall and occurrence of blebs in new pole daughter cells. (A) WT Msm stained with Alexa Fluor™ 488 NHS ester, washed and visualized over time. New material is unstained, old material is stained green. Orange arrows indicate a new pole. Orange stars mark new pole daughter cells. All scale bars=5µm **(B)** Maximum cell width of ΔLDT cell

lineages over time. Width of new pole daughters = blue circle; width of old pole daughters = orange circle. Division signs denote a division event. At each division, there are two arrows from the dividing cell leading to the resulting new and old pole daughter cell widths (blue and orange respectively).

Fig. S6

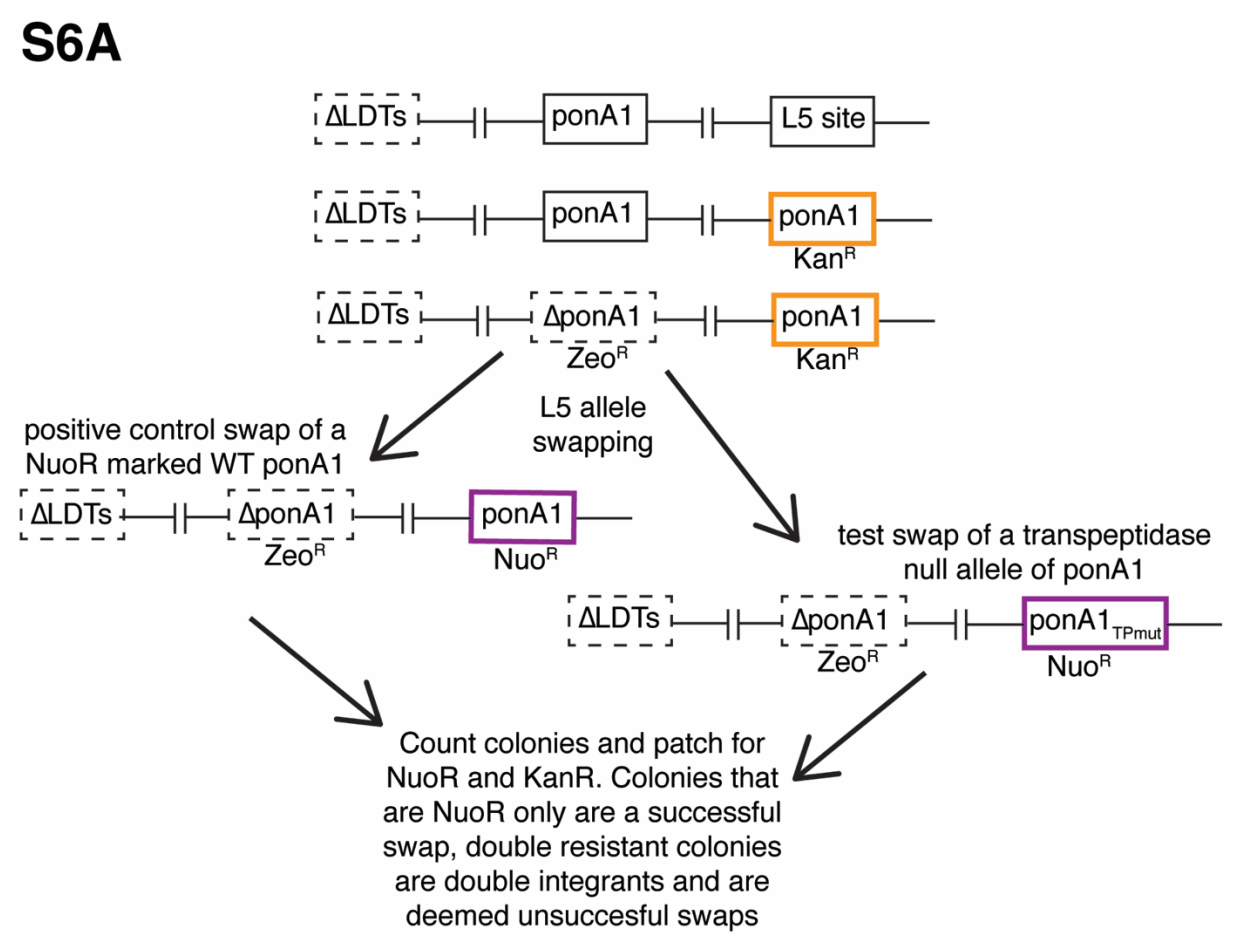

S6B

Genetic Background: ΔLDT ΔponA1 //L5 TetO-ponA1 WT (KanR)	Number of colonies	Proportion of true swaps
SWAP: L5 TetO-ponA1 WT (NuoR)	249	26/50
SWAP: L5 TetO-ponA1 TP mutant (NuoR)	0	

Figure S6: L5 allele swapping to test essentiality of PonA1's ability to form 4-3 crosslinks (transpeptidation). (A) Schematic of L5 allele swapping experiment. Adapted from (*12*). **(B)** Results of *ponA1* allele swapping experiment in ΔLDT cells.

Fig. S7

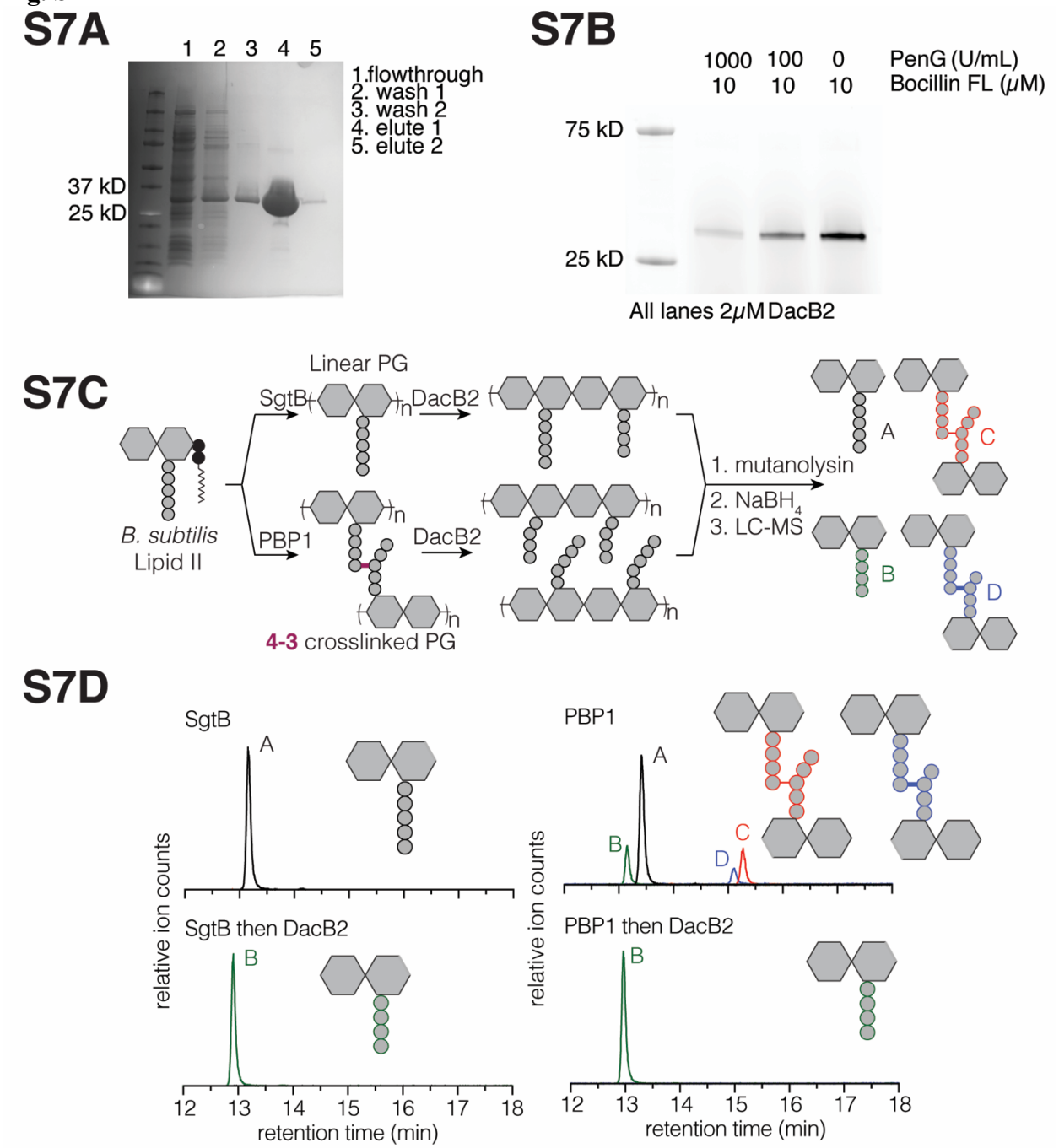

Figure S7: MSMEG_2433 (DacB2) functions as a D,D-carboxypeptidase and D,D-endopeptidase *in vitro*. (A) Coomassie-stained gel of purified His_6-DacB2. **(B)** Bocillin-FL and Penicillin G binding assay of purified DacB2. **(C)** Schematic of *in vitro* experiment to test D,D-carboxy- and D,D-endopeptidase activity. Lipid II extracted from *B. subtilis* is first polymerized into linear (using SgtB) or crosslinked (using *B. subtilis* PBP1) peptidoglycan and then reacted with DacB2. The reaction products are analyzed by LC-MS. **(D)** Extracted ion chromatograms of the reaction products produced by incubation of DacB2 with peptidoglycan substrates.

Fig. S7 (Continued)

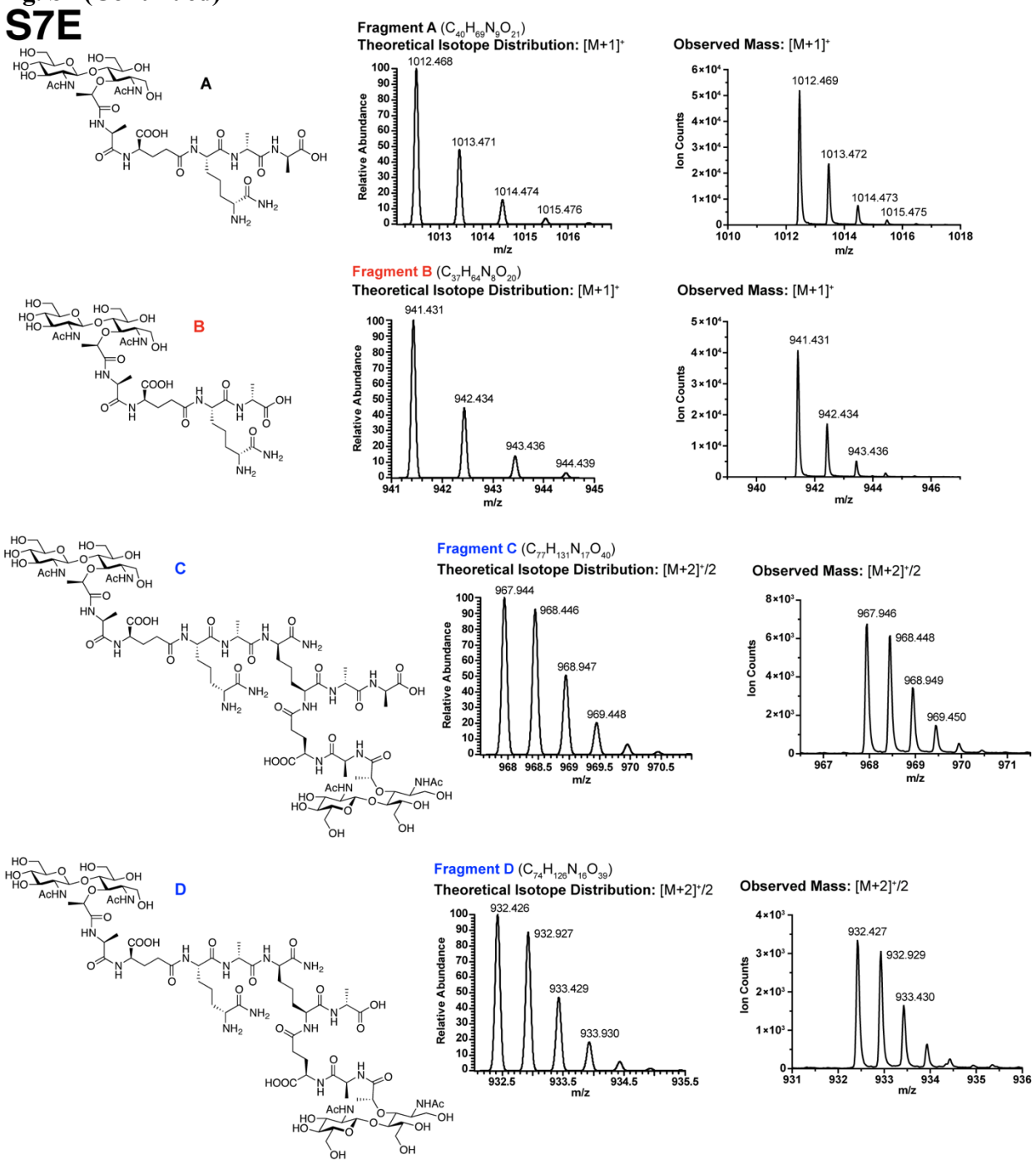

Figure S7 (continued): MSMEG_2433 (DacB2) functions as a D,D-carboxypeptidase and D,D-endopeptidase *in vitro*. (E) Mass spectra of the reaction products of DacB2 digestion reactions.

Fig. S8

S8A

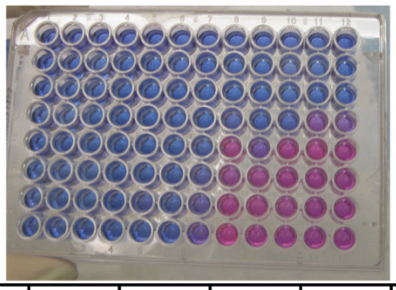

	1	2	3	4	5	6	7	8	9	10	11	12
	10.00	10.00	10.00	10.00	10.00	10.00	10.00	10.00	10.00	10.00	10.00	
A	10.00	5.00	2.50	1.25	0.63	0.31	0.16	0.08	0.04	0.02	0.01	
	5.00	5.00	5.00	5.00	5.00	5.00	5.00	5.00	5.00	5.00	5.00	
B	10.00	5.00	2.50	1.25	0.63	0.31	0.16	0.08	0.04	0.02	0.01	
	2.50	2.50	2.50	2.50	2.50	2.50	2.50	2.50	2.50	2.50	2.50	
C	10.00	5.00	2.50	1.25	0.63	0.31	0.16	0.08	0.04	0.02	0.01	
	1.25	1.25	1.25	1.25	1.25	1.25	1.25	1.25	1.25	1.25	1.25	
D	10.00	5.00	2.50	1.25	0.63	0.31	0.16	0.08	0.04	0.02	0.01	
	0.63	0.63	0.63	0.63	0.63	0.63	0.63	0.63	0.63	0.63	0.63	
E	10.00	5.00	2.50	1.25	0.63	0.31	0.16	0.08	0.04	0.02	0.01	
	0.31	0.31	0.31	0.31	0.31	0.31	**0.31**	0.31	0.31	0.31	0.31	
F	10.00	5.00	2.50	1.25	0.63	0.31	**0.16**	0.08	0.04	0.02	0.01	
	0.16	0.16	0.16	0.16	0.16	0.16	0.16	0.16	0.16	0.16	0.16	
G	10.00	5.00	2.50	1.25	0.63	0.31	0.16	0.08	0.04	0.02	0.01	
	0.08	0.08	0.08	0.08	0.08	0.08	0.08	0.08	0.08	0.08	0.08	
H	10.00	5.00	2.50	1.25	0.63	0.31	0.16	0.08	0.04	0.02	0.01	

S8B

	1	2	3	4	5	6	7	8	9	10	11	12	
A	40.00	20.00	10.00	5.00	2.50	1.25	**0.63**	0.31	0.16	0.08	0.04	0.02	
													amoxicillin
B	40.00	20.00	10.00	5.00	2.50	1.25	**0.63**	0.31	0.16	0.08	0.04	0.02	
C	40.00	20.00	10.00	5.00	2.50	**1.25**	0.63	0.31	0.16	0.08	0.04	0.02	
													meropenem
D	40.00	20.00	10.00	5.00	2.50	**1.25**	0.63	0.31	0.16	0.08	0.04	0.02	

Figure S8: Minimum inhibitory concentration (MIC) of amoxicillin or meropenem alone or in combination against *Mycobacterium tuberculosis*. (A) Resazurin MIC plate and dilution

matrix of amoxicillin and meropenem in combination in a checkerboard MIC plate. The table below shows the concentration of each drug per well in μg/mL. The concentration of meropenem is in black text and the concentration of amoxicillin is in red text in each well. **(B)** Dilution matrix of amoxicillin or meropenem (alone). The concentrations of drugs are shown in the table. Pink indicates metabolically active cells, blue indicates not metabolically active. In both single drug and checkerboard MIC plates, 5μg/mL clavulanate was used.

Fig. S9

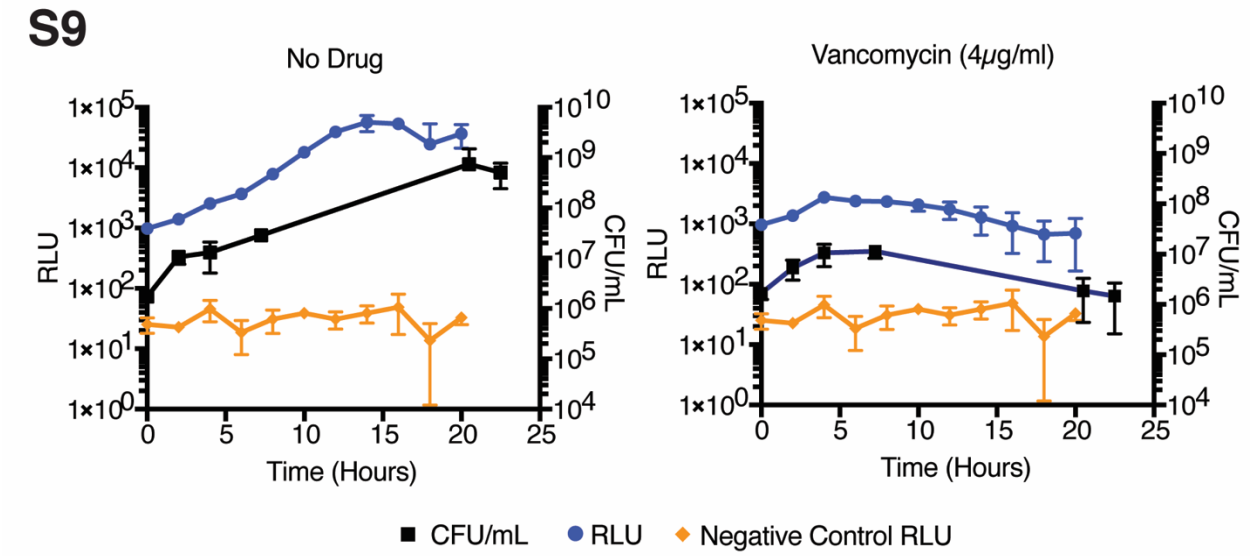

Figure S9: Light production (RLU) correlated to colony forming units (CFU) in mycobacterial cells expressing *luxABCD* in drug treatment. (A) *Mycobacterium smegmatis* colony forming units (CFU) and luminescence (RLU) during drug treatment.

Fig. S10

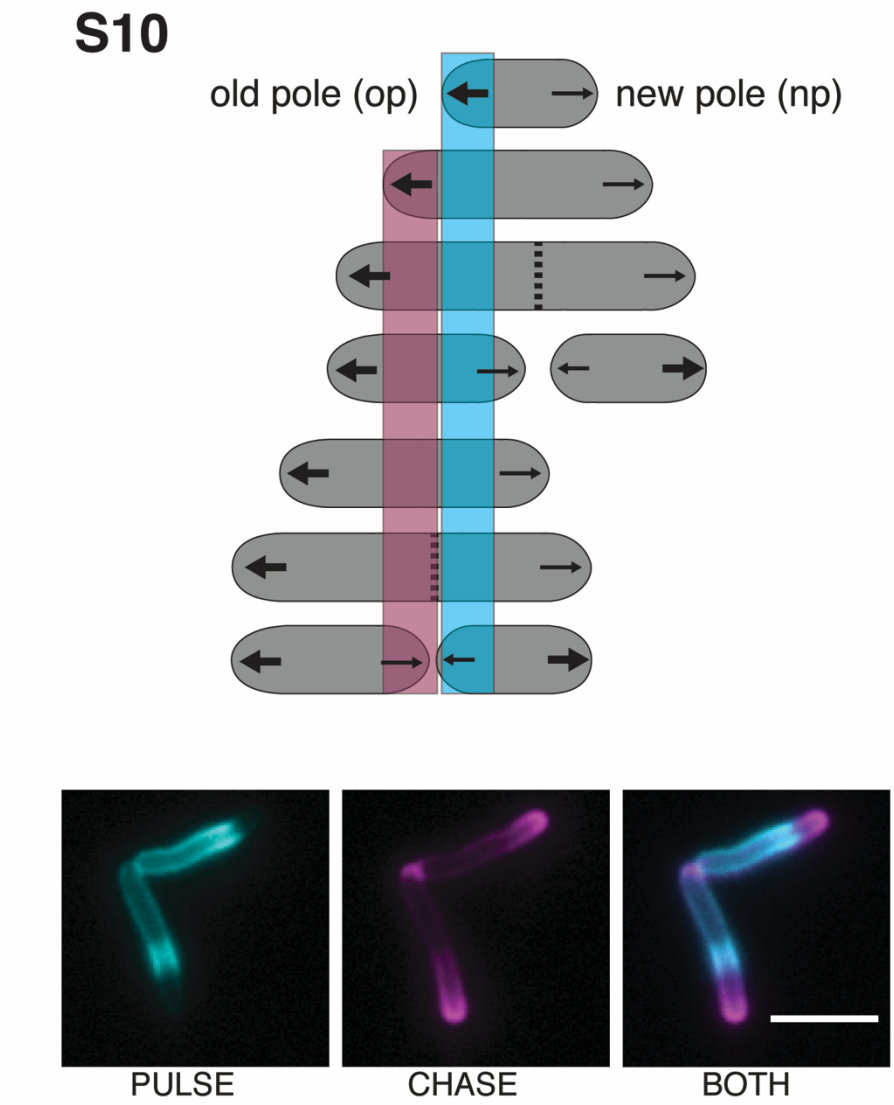

Figure S10: New and old cell wall are spatially segregated in mycobacteria. 2-minute FDAA pulse (cyan), 45-minute outgrowth, followed by 2-minute FDAA chase (magenta) in WT *Mycobacterium smegmatis* cells. Newest cell wall (magenta), older cell wall (cyan). Scale bar=5µm

Table S1: List of Primers

Primer description	Primer Sequence	5' or 3' features	Primer #
MSMEG_3528 (ldtA) upstream flanking region FOR	CGTTGTAAAACGACGGCCAGTGATGGCGGGCGTGATCTGGAATCTCT	pUC57 overlap	208
MSMEG_3528 (ldtA) upstream flanking region REV	ACCCAACTTAATCGCCTTGCAGCTCTTCCAGTGTAGGTTGTCGAAACG	Zeo cassette overlap	209
MSMEG_3528 (ldtA) downstream flanking region FOR	TAATCATGGTCATAGCTGTTTTCATCGTGCAGGCGTGACGTGCAG	Zeo cassette overlap	210
MSMEG_3528 (ldtA) downstream flanking region REV	CAGTCGACGGGCCCGGGATCCGCGGTGGTGCCCTTGGTGATGGTC	pUC57 overlap	211
MSMEG_0233 (ldtE) upstream flanking region FOR	CGTTGTAAAACGACGGCCAGTGGCTGTCCGCCCAGCCCCGGGCC	pUC57 overlap	220
MSMEG_0233 (ldtE) upstream flanking region REV	CCAACTTAATCGCCTTGCAGCGTGGTACCTCCAGAGCACAACTG	Zeo cassette overlap	221
MSMEG_0233 (ldtE) downstream flanking region FOR	GTAATCATGGTCATAGCTGTTTCCGGACGTCATACGAAGAACCCCC	Zeo cassette overlap	222
MSMEG_0233 (ldtE) downstream flanking region REV	GCAGTCGACGGGCCCGGGATCTGGACCGACGCCGACCGCACCG	pUC57 overlap	223
MSMEG_4745 (ldtB) upstream flanking region FOR	GGTCGAGATGCTCCTGGAAGAGGCCG		444
MSMEG_4745 (ldtB) upstream	GAGCTCCAATTCGCCCTACGTCGTTACCTGCCCCATCACG	hyg cassette overlap	445

flanking region REV			
MSMEG_4745 (ldtB) downstream flanking region FOR	GTACCTCGAGTCTAGAAGTAGCGCTATCGCACCGCGCGGTCCAG	hyg cassette overlap	446
MSMEG_4745 (ldtB) downstream flanking region REV	CGACCCGGCCCGTCACAAGGACACCGAAC		447
MSMEG_0929 (ldtC) upstream flanking region FOR	CGTTGTAAAACGACGGCCAGTGAACTGGCGACGGCGCTGGGCGTGG	pUC57 overlap	216
MSMEG_0929 (ldtC) upstream flanking region REV	TGGAGCTCCAATTCGCCCTAGTGGATCTAGGGTACCGACAGCACGC	hyg cassette overlap	448
MSMEG_0929 (ldtC) downstream flanking region FOR	GGTACCTCGAGTCTAGAAGTAGTCCGGCGGCTAGGTCCGGCGGTTGAAG	hyg cassette overlap	449
MSMEG_0929 (ldtC) downstream flanking region REV	CAGTCGACGGGCCCGGGATCCCAAGGGACTCGCGCCGGTCTCC	pUC57 overlap	219
MSMEG_0929 (ldtC) upstream flanking region FOR	GGCTCGTTCTTCACCAACC		507
MSMEG_0929 (ldtC) downstream flanking region REV	CTGCCCAAGCTCATCGAC		508
MSMEG_0674 (ldtG) upstream flanking region FOR	GTTGTAAAACGACGGCCAGTGCGGCGTCGACCTCCCGGCCGGGTC	pUC57 overlap	228
MSMEG_0674 (ldtG) upstream flanking region REV	GTGGAGCTCCAATTCGCCCTAGCGCATTGGCTTCCGATTTCCCTCG	hyg cassette overlap	454

MSMEG_0674 (ldtG) downstream flanking region FOR	CGGTACCTCGAGTCTAGAAGTACGCCGACGTGTATGCCCACCCCCGCG	hyg cassette overlap	455
MSMEG_0674 (ldtG) downstream flanking region REV	GCAGTCGACGGGCCCGGGATCGCCTGCGCCCGCGGGAGCGCCTGCC	pUC57 overlap	231
MSMEG_0674 (ldtG) upstream flanking region FOR	GCATCTGAGTTTCGGCAAG		513
MSMEG_0674 (ldtG) downstream flanking region REV	CAACTACCCCGCAGTTGAAT		514
MSMEG_1322 (ldtF) upstream flanking region FOR	GTTGTAAAACGACGGCCAGTGCGAGGTAAGGGTCTCGACGGTTTCT	pUC57 overlap	224
MSMEG_1322 (ldtF) upstream flanking region REV	GTGGAGCTCCAATTCGCCCTATCCAATGTGCTTCGGCGAAAGCCAGTTTG	hyg cassette overlap	452
MSMEG_1322 (ldtF) downstream flanking region FOR	GTACCTCGAGTCTAGAAGTAGTTCCCCCCGGCCCACATATGTCTGGACG	hyg cassette overlap	453
MSMEG_1322 (ldtF) downstream flanking region REV	GCAGTCGACGGGCCCGGGATCCACGACAACGCCAGCGCGAT	pUC57 overlap	227
MSMEG_1322 (ldtF) upstream flanking region FOR	GGTCGACGACGAACTGGT		511
MSMEG_1322 (ldtF) downstream flanking region REV	AACGGCACGTACATCAGGAC		512

MSMEG_0233 (ldtE) FOR with TetO overlap (vector)	CATGCTTAATTAAGAAGGAGATATACAATGCCGAAATCGGCAAAACGCAG		323A
MSMEG_0233 (ldtE) REV (no stop codon) with ser-ser-gly linker	GATGACGTCCTCGGAGGAGGCCGAGCCGCCGAACATCTGCCAGTCGGATG		351
mRFP FOR with ser-ser-gly linker	CATCCGACTGGCAGATGTTCGGCGGCTCGGCCTCCTCCGAGGACGTCATC		352
mRFP REV with vector overlap	GTCCCCAATTAATTAGCTAAGTGATGGTGATGGTGATGACAGGCG		353
MSMEG_2433 (dacB2) FOR (first 27 amino acids truncated)	GGCCTGGTGCCGCGCGGCAGCCATCGCGCGGACGCCGACATCCAG	with 5' overlaps to pet28b cut with NdeI	662
MSMEG_2433 (dacB2) REV	GCTGTCCACCAGTCATGCTAGCCATCAGAGCGCCCCGATGCTCG	with 3' overlaps to pet28b cut with NdeI	663

Table S2: List of Strains

Strain	Description	Primers
KB134	mc2155Δ*ldtA*::loxP	208/209; 210/211
KB156	mc2155Δ*ldtA*::loxP + Δ*ldtE*:: zeoR	220/221; 222/223
KB200	mc2155Δ*ldtA*::loxP Δ*ldtE*:: zeoR + Δ*ldtB*:: hygR	444/445; 446/447
KB209	mc2155Δ*ldtA*::loxP Δ*ldtE*::loxP Δ*ldtB*::loxP + Δ*ldtC*:: hygR	216/448; 449/219 (create original hyg KO) but used 507/508; (amplify KO from strain within the flanks)
KB222	mc2155Δ*ldtA*::loxP Δ*ldtE*::loxP Δ*ldtB*::loxP Δ*ldtC*:: hygR Δ*ldtG*:: zeoR	228/454; 455/231 (create original hyg KO) but used 513/514; (amplify KO from strain within the flanks)
KB303 (ΔLDT)	mc2155Δ*ldtA*::loxP Δ*ldtE*::loxP Δ*ldtB*::loxP Δ*ldtC*:: loxP Δ*ldtG*:: loxP Δ*ldtF*:: hygR	224/452; 453/227 (create hyg KO) but used 511/512 (amplify KO from strain or gibson)
KB302	pTetO-ldtE(MSMEG_0233)-linker-mRFP in CT94 XH (XL1-Blue)	323A/351; 352/353
KB316 (ΔLDTcomp)	[mc2155ΔldtA::loxP ΔldtE::loxP ΔldtB::loxP ΔldtC:: loxP ΔldtG:: loxP ΔldtF:: hygR] + KB302	
KB428	*E.coli* BL21 + pet28b (dacB2)	662/663